Journal of Computational Physics **152,** 756–789 (1999)
Article ID jcph.1999.6262, available online at http://www.idealibrary.com on IDEAL®

New Self-Similar Solutions of the Nonlinear Schrödinger Equation with Moving Mesh Computations[1]

Chris J. Budd,*[,2] Shaohua Chen,† and Robert D. Russell†

*Department of Mathematics, University of Bath, Claverton Down, Bath BA2 7AY, United Kingdom;
†Department of Mathematics and Statistics, Simon Fraser University, Burnaby,
British Columbia V5A 1S6, Canada
E-mail: cjb@maths.bath.ac.uk, schend@cs.sfu.ca, rdr@cs.sfu.ca

Received November 20, 1998

We study the blow-up self-similar solutions of the radially symmetric nonlinear Schrödinger equation (NLS) given by $iu_t + u_{rr} + \frac{d-1}{r}u_r + u|u|^2$, with dimension $d > 2$. These solutions become infinite in a finite time T. By a series of careful numerical computations, partly supported by analytic results, we demonstrate that there is a countably infinite set of blow-up self-similar solutions which satisfy a second order complex ordinary differential equation with an integral constraint. These solutions are characterised by the number of oscillations in their amplitude when d is close to 2. The solutions are computed as functions of d and their behaviour in the critical limit as $d \to 2$ is investigated. The stability of these solutions is then studied by solving the NLS by using an adaptive numerical method. This method uses moving mesh partial differential equations and exploits the scaling invariance properties of the underlying equation. We demonstrate that the single-humped self-similar solution is globally stable whereas the multi-humped solutions all appear to be unstable.

Key Words: nonlinear Schrödinger equation; finite time blow-up; self-similar solutions; adaptive mesh methods.

1. INTRODUCTION

The cubic nonlinear Schrödinger equation (NLS)

$$i\frac{\partial u}{\partial t} + \Delta u + |u|^2 u = 0, \qquad t > 0 \tag{1.1}$$

[1] This work was supported in part by the NSERC (Canada) under Grant OGP-0008781, the Royal Society, and the EPSRC (UK) under Grant GR/J56219.

[2] To whom correspondence should be addressed.

0021-9991/99 $30.00

$$u(\mathbf{x}, 0) = u_0(\mathbf{x}), \qquad \mathbf{x} \in R^d \tag{1.2}$$

describes many physical situations, including phenomena in nonlinear optics and plasma physics (see [Ha89, Za84]). For the well studied case of $d = 1$, the equation is integrable and a solution exists globally. If $d \geq 2$ then for some initial conditions, such as those for which the invariant energy

$$E = \int_{R^d} \left(|\nabla u_0|^2 - \frac{1}{2}|u_0|^4 \right) dx < 0, \tag{1.3}$$

the NLS has solutions that become singular in a finite time T. In this case the solution becomes infinite at a single point at which there is a growing and increasingly narrow peak. In plasma physics, the singularity is usually called a collapse, and in nonlinear optics, the singularity corresponds to an extreme increase of the field amplitude due to self-focusing. There is considerable interest in the nature of the behaviour of this peak and many authors (see [ADKM92, FP98, Fi96, TS92, LPSS88a–LPSS88c, MPSS86]) have investigated the structure of the singularity both numerically and analytically. These investigations have usually considered the case of radially symmetric solutions which are functions of $r = |\mathbf{x}|$ where the singularity occurs at $r = 0$. In an important series of papers, LeMesurier *et al.* [LPSS88a, LPSS88b] and Landman *et al.* [LPSS88c] have used a numerical method derived from rescaling properties of the underlying equation called *dynamic rescaling*. This method has proved successful in both calculating the blow-up rate and giving significant information about the shape of the singularity. In dimension $d = 3$ (and indeed for all $2 < d < 4$ for radially symmetric solutions), the overwhelming evidence is that the solutions blow up in a self-similar way so that there is a function $Q(\xi)$ and a scalar a for which

$$u(r, t) = (2a(T - t))^{-1/2} e^{i\theta + i \log(T/(T-t))/2a} Q(x/(2a(T - t))^{1/2}).$$

Here the function $Q(\xi)$ satisfies an ordinary differential equation with an integral constraint, and the unknown scalar a plays the role of a nonlinear eigenvalue. In contrast, in dimension 2 the numerical and asymptotic evidence is that the blow-up is *approximately* self-similar with

$$\|u\|_\infty \text{ proportional to } \left((T - t)/ \log\log \frac{1}{T - t} \right)^{-\frac{1}{2}}. \tag{1.4}$$

Fibich and Papanicolaou [FP98] confirmed the log log law for $d = 2$ and showed asymptotic equivalence of the adiabatic law of Fibich and Malkin and the loglog law. They also obtained several formulas to approximately calculate the blow-up time T and discussed more general perturbed nonlinear Schrödinger equations. The value of $d = 2$ is a critical point in the analysis of (1.1) with qualitatively differnt behaviour occurring for the three cases of $d < 2$, $d = 2$, and $d > 2$.

In this paper we make a further analysis of the radially symmetric self-similar solutions in the case of $2 < d < 4$. Our principle result will be a numerical demonstration of an infinite number of distinct self-similar solutions which are characterised by the number of maxima of the function $|Q|$ when d is close to 2. These solutions are all parametrised by d and exist when $d = 3$. For this particular value we study their stability by solving the partial differential equation (1.1) numerically. The numerical method used is a development of

the scale invariant moving mesh PDE methods described in [BHR96]. These methods are closely related to dynamic rescaling techniques, but are rather more general and easier to implement. Using these we demonstrate that the blow-up profiles in which $|Q|$ is monotone when $d = 3$ (computed in earlier papers) are globally stable, whereas the multi-bumped profiles represent unstable self-similar solutions.

The layout of the remainder of this paper is as follows. In Section 2 we review some of the existing theory for problem (1.1), derive the ordinary differential equation satisfied by Q, and establish some analytic properties of the solutions. In Section 3 we solve the ordinary differential equation numerically and demonstrate the existence of a countably infinite set of multi-bumped solutions. In Section 4 we describe the underlying theory of the scale invariant moving mesh methods used to compute the solutions of (1.1). In Section 5 we use this method to investigate the stability of the self-similar solutions derived in Section 4. Finally in Section 6 we draw some conclusions from this work.

2. SOME IDENTITIES AND AN EXISTENCE THEOREM FOR THE EQUATION SATISFIED BY THE SELF-SIMILAR SOLUTIONS

If we take $r = |\mathbf{x}|$ and consider radially symmetric solutions of (1.1) only, then these satisfy the partial differential equation

$$i\frac{\partial u}{\partial t} + \frac{\partial^2 u}{\partial r^2} + \frac{d-1}{r}\frac{\partial u}{\partial r} + |u|^2 u = 0, \tag{2.1}$$

where u is complex-valued. For all $t \geq 0$ this partial differential equation has two invariants of evolution which are the mass

$$P = \int_0^\infty |u(r,t)|^2 r^{d-1}\, dr \tag{2.2}$$

and the energy

$$E = \int_0^\infty \left(\left| \frac{\partial u(r,t)}{\partial r} \right|^2 - \frac{1}{2}|u(r,t)|^4 \right) r^{d-1}\, dr. \tag{2.3}$$

A particular class of global solutions of (2.1) is the so-called *waveguide solutions* $u(r,t) = e^{it}R(r)$, where $R(r)$ satisfies

$$R''(r) + \frac{d-1}{r}R'(r) - R(r) + R^3(r) = 0, \qquad R'(0) = 0, \quad R(\infty) = 0. \tag{2.4}$$

Equation (2.4) has a unique, monotonically decreasing and positive solution [MS81] called the *Townes soliton* which plays an important role in the analysis of (2.1) in the limit of $d \to 2$. Using the waveguide solution, one can construct an exact solution of (2.1) which blows up in a finite time T and is of the form

$$u(r,t) = \frac{1}{T-t} R\left(\frac{r}{T-t}\right) \exp\left(-i\frac{r^2/4+1}{T-t}\right).$$

However, this solution is unstable and has not been observed in numerical computations (see [LPSS88b]).

Now, if λ is any real number then Eq. (2.1) is invariant under the transformations

$$u \to e^{i\lambda} u \tag{2.5}$$

or

$$t \to \lambda t, \qquad r \to \lambda^{1/2} r, \qquad u \to \lambda^{-1/2} u. \tag{2.6}$$

Motivated by these invariances we seek blow-up self-similar solutions of (2.1) which take the form

$$u(r,t) = \frac{1}{\sqrt{2a(T-t)}} \exp\left(i\theta + \frac{i}{2a} \log \frac{T}{T-t} \right) Q\left(\frac{r}{\sqrt{2a(T-t)}} \right). \tag{2.7}$$

At this stage a is an undetermined real number and θ is a fixed phase shift. Substituting (2.7) into (2.1) we find that the function $Q(\xi)$ satisfies the following ordinary differntial equation:

$$Q_{\xi\xi} + \frac{d-1}{\xi} Q_\xi - Q + ia(\xi Q)_\xi + |Q|^2 Q = 0, \tag{2.8}$$

$$Q_\xi(0) = 0, \qquad Q(0) = \text{real}, \qquad Q(\infty) = 0. \tag{2.9}$$

The resulting invariants P and E then become

$$P = (T-t)^{(d-2)} \int_0^\infty |Q(\xi)|^2 \xi^{d-1}\, d\xi, \tag{2.10}$$

$$E = (T-t)^{-(4-d)} \int_0^\infty \left(\left| \frac{\partial Q(\xi)}{\partial \xi} \right|^2 - \frac{1}{2} |Q(\xi)|^4 \right) \xi^{d-1}\, d\xi. \tag{2.11}$$

If we define

$$H(Q) \equiv \int_0^\infty \left(\left| \frac{\partial Q(\xi)}{\partial \xi} \right|^2 - \frac{1}{2} |Q(\xi)|^4 \right) \xi^{d-1}\, d\xi, \tag{2.12}$$

then if $2 < d < 4$ and the energy E of the solution is finite, the self-similar solution must have unbounded L_2 norm and satisfy the constraint

$$H(Q) = 0. \tag{2.13}$$

This form for a self-similar solution was given originally in [Za84]. The problem of finding a self-similar solution is thus reduced to finding a function $Q(\xi)$ and a scalar a which together satisfy the ordinary differential equation (2.8), (2.9), and the constraint (2.13). Solutions of this ordinary differential equation for which $|Q|$ is monotone decreasing have been calculated in [LPSS88b], and it has been reported that the equation with the constraint has a unique solution. These numerical calculations imply that as $d \to 2$ we have $a \to 0$ and $Q \to R$. An existence proof together with a demonstration of local uniqueness for both the function $Q(\xi)$ and a in the limit of $d \to 2$ is given in [KL95]. Numerical calculations using the dynamic rescaling method when $d = 3$, strongly imply that the monotone decreasing solution represents a globally attracting form of behaviour, so that the blow-up solutions of

the initial value problem when rescaled tend towards the function $Q(\xi)$ from a variety of initial states.

In this paper we give numerical evidence which implies that problem (2.8), (2.9), and (2.13) has an infinite number of solutions for which $|Q(\xi)|$ is non-monotone and which under transformation are unstable blow-up solutions.

We first obtain some useful identities and obtain the decay rate for the solutions of (2.8) for $2 < d < 4$. Wang [W90] proved that the initial value problem (2.8) and (2.9) has a solution $Q(\xi)$ with $|Q(\xi)| \le c\xi^{-1}$ for any a when $d = 3$. We show that this result can be generalized for any $d > 2$. In fact, we can prove that, for any $d > 2$, $a > 0$, and $Q(0)$, problem (2.8) and (2.9) has a unique solution.

LEMMA 2.1. *If $Q(\xi)$ is a solution of* (2.8) *and* (2.9), *then*

$$|\xi Q' + Q|^2 + \frac{1}{2}\xi^2|Q|^4 + \int_0^\xi s|Q(s)|^4\,ds$$

$$= (d-2)|Q(0)|^2 + \xi^2|Q|^2 + (3-d)|Q|^2 + 2(3-d)\int_0^\xi s|Q'(s)|^2\,ds, \quad (2.14)$$

$$2\xi\,\mathrm{Im}(Q'\bar{Q}) + 2(d-2)\int_0^\xi \mathrm{Im}(Q'\bar{Q})\,ds + a\xi^2|Q(\xi)|^2 = 0, \quad (2.15)$$

and

$$\xi^d|Q'|^2 - \frac{2}{a}\xi^{d-1}\mathrm{Im}(Q'\bar{Q}) + \frac{1}{2}\xi^d|Q|^4 + 2\xi^{d-1}\mathrm{Re}(Q'\bar{Q})$$

$$= (4-d)\int_0^\xi \left(|Q'(s)|^2 - \frac{1}{2}|Q(s)|^4\right)s^{d-1}\,ds. \quad (2.16)$$

Proof. Multiplying (2.8) by $2\xi^k(\xi\bar{Q}' + \bar{Q})$ with $k = 1$ and $k = d-1$, respectively, taking real parts and integrating the results gives (2.14) for $k = 1$ and

$$\xi^d|Q'|^2 - \xi^d|Q|^2 + \frac{1}{2}\xi^d|Q|^4 + 2\xi^{d-1}\mathrm{Re}(Q'\bar{Q}) - (4-d)$$

$$\int_0^\xi \left(|Q'(s)|^2 - \frac{1}{2}|Q(s)|^4\right)s^{d-1}\,ds + (d-2)\int_0^\xi s^{d-1}|Q(s)|^2\,ds = 0 \quad (2.17)$$

for $k = d-1$. Similarly, multiplying (2.8) by $2\xi^k\bar{Q}$ with $k = 1$ and $k = d-1$, respectively, taking imaginary parts, and integrating the results give (2.15) for $k = 1$ and

$$a(d-2)\int_0^\xi s^{d-1}|Q(s)|^2\,ds = a\xi^d|Q(\xi)|^2 + 2\xi^d\mathrm{Im}(Q'\bar{Q}) \quad (2.18)$$

for $k = d-1$. Finally, substituting (2.18) into (2.17) gives (2.16). ∎

THEOREM 2.2. *If $2 < d < 4$, then for any given initial value $Q(0)$ and constant $a > 0$, problem* (2.8) *and* (2.9) *has a unique solution. Furthermore, $|Q(\xi)| \le c\xi^{-1}$ and $|Q'(\xi)| \le c\xi^{-\alpha}$ for large ξ, where $\alpha = 1$ if $d \ge 3$ and $0 < \alpha < d-2$ if $d < 3$.*

Proof. The problem is equivalent to the following integral equation:

$$Q(\xi) = Q(0) - ia\int_0^\xi sQ(s)\,ds + \frac{1}{d-2} \times \int_0^\xi [(1+iad-ia) - |Q(s)|^2]Q(s)\left(s - \frac{s^{d-1}}{\xi^{d-2}}\right)ds, \qquad Q(\infty) = 0. \quad (2.19)$$

From the theory of Volterra integral equations (see [Bu83]), (2.19) has a unique local solution and can be extended to $\xi = \infty$ if $|Q(\xi)|$ is bounded.

Now it suffices to prove that $|Q| \le c\xi^{-1}$ and $|Q'(\xi) \le c\xi^{-\alpha}$. Rewrite (2.14) as

$$\begin{aligned}(1-\delta)|Q'|^2 + \delta\left|Q' + \frac{Q}{\delta\xi}\right|^2 + |Q|^2\left(\frac{1}{2}|Q|^2 - 1\right) \\ -\frac{1}{\xi^2}\left(\frac{1}{\delta} + d - 2\right)|Q|^2 + \frac{1}{\xi^2}\int_0^\xi s|Q(s)|^4\,ds \\ = \frac{d-2}{\xi^2}|Q(0)|^2 + \frac{2(3-d)}{\xi^2}\int_0^\xi s|Q'(s)|^2\,ds, \end{aligned} \quad (2.20)$$

where $0 < \delta < d-2$. From this identity we see that if $|Q'|$ is bounded so is $|Q|$. Suppose that $|Q'|$ is unbounded. Then there exists a monotone sequence ξ_j such that $|Q'(\xi_j)| \to \infty$ as $\xi_j \to \infty$ and $|Q'(\xi_j) \ge |Q'(\xi)|$ for $\xi_j \ge \xi$. From (2.20),

$$(1-\delta)|Q'(\xi_j)|^2 \le c + \frac{2(3-d)}{\xi_j^2}\int_0^{\xi_j} s|Q'(s)|^2\,ds \le c + (3-d)|Q'(\xi_j)|^2,$$

which is a contradiction as $j \to \infty$. Hence $|Q|$ and $|Q'|$ are bounded. By (2.15) we have

$$a\xi^2|Q(\xi)|^2 \le c\xi,$$

which implies $|Q(\xi)| \le c\xi^{-1/2}$. Successively substituting this and updated estimates into (2.15) we obtain

$$|Q(\xi)| \le c\xi^{-1+\varepsilon}, \quad (2.21)$$

where $0 \le \varepsilon < d-2$. Multiplying (2.20) by $\xi^{2\alpha}$ with $0 < \alpha < (d-2)/(1-\delta)$ we have

$$(1-\delta)\xi^{2\alpha}|Q'|^2 \le c + \frac{2(3-d)}{\xi^{2-2\alpha}}\int_0^\xi s|Q'(s)|^2\,ds \le c + \frac{3-d}{1-\alpha}\max_{0\le s\le\xi} s|Q'(s)|^2,$$

which implies that if $d < 3$ then $\xi^{2\alpha}|Q'|^2 \le c$ by a similar argument as before. Substituting this inequality and (2.21) into (2.15) we obtain $|Q| \le c\xi^{-1}$.

If $d \ge 3$, we obtain $|Q'| \le c\xi^{-1}$ directly from (2.14). ■

LEMMA 2.3. *Suppose that Q is a solution of* (2.8) *and* (2.9) *and $2 < d < 4$, then $H(Q) = 0$ iff*

$$\left|\xi Q' + \left(1 + \frac{i}{a}\right)Q\right| \to 0 \qquad \text{as } \xi \to \infty. \quad (2.22)$$

Proof. Rewrite (2.16) as

$$\xi^{d-2}\left|\xi Q' + \left(1+\frac{i}{a}\right)Q\right|^2 + \frac{1}{2\xi^{4-d}}\left[\xi^2|Q|^2 - \left(1+\frac{1}{a^2}\right)\right]^2 - \left(1+\frac{1}{a^2}\right)^2\frac{1}{\xi^{4-d}}$$
$$= (4-d)\int_0^\xi \left(|Q'(s)|^2 - \frac{1}{2}|Q(s)|^4\right)s^{d-1}\,ds, \tag{2.23}$$

and the conclusion follows on letting $\xi \to \infty$. ■

3. A PLETHORA OF MULTI-BUMP SELF-SIMILAR SOLUTIONS

From Theorem 2.2 in Section 2 we have that the initial value problem consisting of (2.8), $Q'(0) = 0$, and $Q(0)$ given has a unique global solution such that $|Q(\xi)| \to 0$ as $\xi \to \infty$. The solutions of the initial value problem which correspond to self-similar solutions of the partial differential equation satisfy the integral identity (2.13), and from Lemma 2.3 we see that this is equivalent to the point condition (2.22).

An alternative derivation of this result follows from the observation that for large ξ, there are constants α and β which depend upon the initial conditions and for which $Q(\xi)$ is asymptotic to

$$Q(\xi) \sim \alpha\xi^{-1}\exp\left(-\frac{i}{a}\log(\xi)\right) + \beta\xi^{-(d-1)}\exp\left(-\frac{ia\xi^2}{2} + \frac{i}{a}\log(\xi)\right). \tag{3.1}$$

Observe that this comprises a slowly oscillating solution added to a more rapidly decaying, but rapidly oscillating component. A simple calculation then implies that when ξ is large the leading order contribution to (2.22) is given by

$$\left|\xi Q_\xi + \left(1+\frac{i}{a}\right)Q\right|^2 = |\beta|^2 a^2 \xi^{6-2d}, \tag{3.2}$$

and hence the solutions of (2.8), (2.9), and (2.22) are precisely those which oscillate slowly as $\xi \to \infty$ if $|\beta| = 0$.

We present numerical evidence which strongly indicates that there are an *infinite* number of multi-bump non-zero solutions of (2.8), (2.9), and (2.22). These lie on solution branches parametrised by d such that as $d \to 2$, $a \to 0$ on each branch and either $Q(0) \to 0$ or $Q(0) \to 2.20620086465$ which is the value at $\xi = 0$ of the ground state solution $R(\xi)$. The branches are characterised by the number of oscillations of the function $|Q(\xi)|$ and are reminiscent of the multi-bump homoclinic solutions of real fourth order ordinary differential equations derived by Buffoni, Champneys, and Toland [CT93, BCT96]. The branch identified by Papanicolaou and co-workers in [LPSS88b] is that for which the function $|Q(\xi)|$ is *monotone decreasing* in ξ when d is close to 2.

3.1. *Numerical Methods*

We use two numerical methods to solve the system (2.8), (2.9), and (2.22). The first, based upon a shooting method, is robust in the sense that it will find a solution given a fairly poor initial guess for $Q(0)$ and a. The second, based upon collocation, requires a good initial guess for $Q(\xi)$ but is significantly faster and more accurate. Typically, we use it to

follow a branch of solutions as d varies, once a starting solution on the branch has been found by the shooting method.

First we describe the shooting method. Consider the initial value problem (2.8) with given real a and $\gamma \equiv Q(0)$. This has a solution $Q(\xi, a, \gamma)$ valid for all ξ. This solution can be constructed relatively easily using a standard ordinary differential equation solution method. As the slowly varying solution we are seeking is close to highly oscillatory solutions, it is important that it be approximated well. This requires the use of a stiff solver with high error tolerance. Accordingly, we use a BDF method with relative tolerance of 10^{-14} to solve the initial value problem.

Using this we solve for $Q(\xi)$ in the range $0 \le \xi \le X$ for a suitably large X and calculate the function

$$F(X, a, \gamma) \equiv |XQ_\xi + (1 + i/a)Q(X)|^2. \tag{3.3}$$

To enforce the condition that $\beta = 0$ we approximate the condition that

$$F(X, a, \gamma) \to 0 \qquad \text{as } X \to \infty \tag{3.4}$$

by taking X large and finding values of a and γ such that

$$F(X, a, \gamma) = 0.$$

This introduces an error which we shall show presently is small provided that X is sufficiently large. Setting $F = 0$ is equivalent to finding a (local) minimum of F over a range of values of a and γ. According to the theory presented in [KL95], the solutions of (2.8), (2.9), and (2.22) are *locally* unique. Such points lead to values of a and γ which are local minimisers of $F(X, a, \gamma)$. We define such points to be $(A(X), \Gamma(X))$, and each such point leads to a solution of (2.8), (2.9), and (2.22) provided that F is zero at the local minimum and $A(X), \Gamma(X)$ have limiting values as $X \to \infty$. Whereas earlier calculations reported in [KL95], LPSS88b] claim uniqueness for the values $A(X), \Gamma(X)$ in the limit of $X \to \infty$ we believe there to be an infinite number of such isolated points. To determine them we use the following algorithm:

ALGORITHM 1.

- Set X large (typically X is in the range of 200 to 1000).
- Take an initial guess (a, γ) for $(A(X), \Gamma(X))$.
- Starting from the initial guess, find a local minimiser $(A(X), \Gamma(X))$ for F.
- Increase X and repeat till convergence.

To perform the minimisation, we used a Broyden method (the NAG routine E04JAF) which performed robustly for a variety of initial guesses. Indeed, this procedure proved far more robust to errors in the initial guess than using a nonlinear solver to find the zeros of F. Typically the minimisation terminated when $F < 10^{-15}$.

The values of $A(X), \Gamma(X)$ so derived converge rapidly as the value of X increases which makes the procedure reasonably quick to implement. To see this, we continue the estimation of the slowly varying solution $Q(\xi)$ for large ξ. A simple calculation shows that there is a constant K which depends upon a and α such that

$$Q(\xi) \sim \alpha\xi^{-1} \exp\left(-\frac{i}{a}\log(\xi)\right)\left(1 + \frac{K}{\xi^2}\right) + \beta\xi^{-(d-1)} \exp\left(-\frac{ia\xi^2}{2} + \frac{i}{a}\log(\xi)\right). \tag{3.5}$$

(It can be shown that when a is small, K is inversely proportional to a^2.) Using (3.5) we can further estimate F to give

$$F(X,a,\gamma) \sim \left| -ia\beta X^{2-(d-1-i/a)} \exp\left(-\frac{iaX^2}{2}\right) + \frac{K\alpha}{X^3}\left(1+\frac{i}{a}\right)\exp\left(-\frac{i}{a}\log(X)\right)\right|^2.$$

We see from this estimate that if $F=0$ then

$$|\beta| \sim \frac{K\alpha}{a} X^{d-6}.$$

Observe that the resulting value of β is non-zero, but provided $d<6$, β diminishes rapidly as we increase X. From this calculation we can estimate the resulting errors in $A(X)$ and $\Gamma(X)$. Suppose that $(A(X),\Gamma(X)) \to (A,\Gamma)$ as $X\to\infty$. If $A(X)-A$ and $\Gamma(X)-\Gamma$ are both small then from the standard theory for initial value problems, we have that β is proportional to both $A(X)-A$ and $\Gamma(X)-\Gamma$. Indeed, numerical experiments strongly imply that the constant of proportionality is in both cases independent of the value of X. From this we deduce that the error introduced by estimating A and Γ at a finite value of X is also proportional to X^{d-6} for large X. This result has been supported by some simple numerical experiments.

While the shooting method coupled with the minimisation of the function F is reasonably robust with respect to the initial values, it still requires an initial guess to start it off. This initial guess has to be reasonably close to the correct solution to prevent the highly oscillatory part of the solution from dominating the slowly varying component and making minimisation of F impossible. Empirically, the starting values of a and γ have to be within 5% of the correct values to give convergence. To obtain this initial guess we note from the results in [KL95] that as $d\to 2$ we have $a\to 0$. Setting $a=0$ and $d=2$ in Eq. (2.8) gives

$$R_{\xi\xi}+\frac{1}{\xi}R_\xi - R + R|R|^2 = 0, \qquad R_\xi(0)=0, \qquad R(0) \text{ real}, \qquad R\to 0 \text{ as } \xi\to\infty. \quad (3.6)$$

It is well known that this equation has a unique positive solution (called the *ground state* [MS81]) which decays exponentially for large ξ. Indeed, there are a discrete set of values of $R(0)$ at which it has a solution, with the first three (in increasing order) given by

$$\gamma_0 = 0, \qquad \gamma_1 = 2.20620086465, \qquad \gamma_2 = 3.33198926658.$$

Here the ground state is given by γ_1. The solution of (2.8) for which $|Q|$ is monotone decreasing determined in [LPSS88b] is known to be a perturbation of the ground state with $Q(0)$ close to γ_1 when d is close to 2. To seek more solutions we take d close to 2 and search for values of (A,Γ) in a neighbourhood of each of the points $(0,\gamma_i)$. In particular, taking $d=2.01$ we found many solutions with Γ close to both 0 and to γ_1, although none were found close to γ_2 or to larger values. These solutions served as the starting points of our branch calculation, and each gave rise to a branch, classified by the number of oscillations of $|Q|$, which were extended either forward to $d=4$ or backward to $d=2$.

Calculating the branches. Once the first point of a solution branch has been determined it is possible to find subsequent points by using pseudo-arclength continuation as described by Keller [Ke93]. This method uses a predictor corrector procedure to find points on the

branch, in which values of a, γ, and of the function $Q(\xi)$ are predicted from previous solution values on the branch, and these values are then corrected using a nonlinear solver. As the predicted values are close to the final values the nonlinear solver does not have to be as robust as the methods used to get onto the branch, but instead it needs to be fast at calculating a large number of points on the branches. To do this we used the following algorithm:

ALGORITHM 2.

- Set X suitably large.
- For each new value of d along a branch, construct an initial guess for the value of a and of the function $Q(\xi)$, using interpolation from the previous solutions.
- Using the initial guess, solve the coupled two-point boundary value problem

$$Q_{\xi\xi} + \frac{d-1}{\xi} Q_\xi - Q + ia(\xi Q)_\xi + Q|Q|^2 = 0, \qquad a_\xi = 0,$$

with boundary conditions

$$Q_\xi(0) = 0, \qquad \mathrm{Im}(Q(0)) = 0, \qquad XQ_\xi(X) + (1 + i/a)Q(X) = 0.$$

If necessary, increase X to obtain convergence.

The two-point boundary value problems are solved using a spline collocation procedure. In particular, we use the code COLSYS [ACR81] with its continuation option. The code is known for its ability to solve stiff problems, characterized by extreme boundary or interior layers (and for which initial value methods tend to be extremely sensitive). COLSYS uses an adaptive mesh procedure and can treat directly BVPs expressed as mixed-order systems. As a starting guess for the solution on a branch, we use the solution $Q(\xi)$ obtained using the shooting method for $d = 2.01$. As a check on this solution it is recalculated using COLSYS with the shooting method solution as an initial guess. The resulting two solutions were found to be almost indistinguishable. To see the phenomena of slow oscillating and fast oscillating solutions, we plot the real part of the function $Q'(\xi)$ for $0 \le \xi \le 160$ in Fig. 3.1. The dotted line is obtained by the shooting method with $a = 0.166125$ and $Q(0) = 0.0509$. The solid line is obtained by COLSYS with $a = 0.166124963$ and $Q(0) = 0.050957837$.

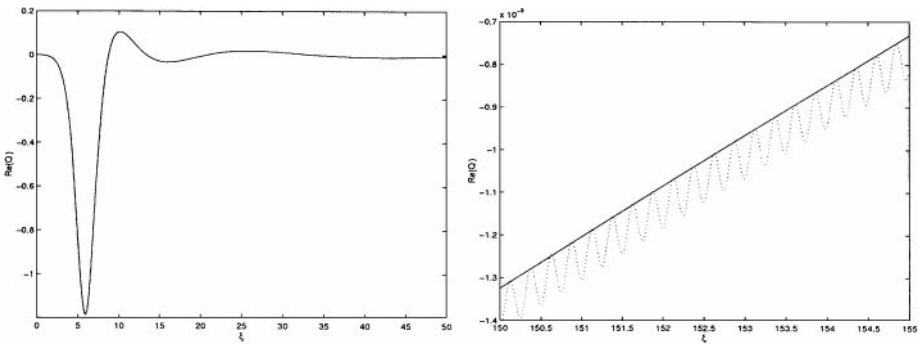

FIG. 3.1. The two curves are almost the same on the left, but the dotted line oscillates faster on the right after enlargement.

TABLE 3.1
Branches Bifurcating from Zero

Γ	A	(m, n)
0.050957837	0.166124963	(0, 1)
0.067775686	0.112487547	(0, 2)
0.083801453	0.085818517	(0, 3)
0.099987189	0.069519523	(0, 4)
0.116433882	0.058454538	(0, 5)
0.133094235	0.050430462	(0, 6)
0.399602580	0.014988764	(0, 23)

3.2. *Results*

In the calculations two distinct families of multiple solution branches were determined which either bifurcate at $d = 2$ from the zero solution $(A, \Gamma) = (0, 0)$ or from the ground state solution $(A, \Gamma) = (0, \gamma_1)$. All of these solution branches bifurcating from $(0, 0)$ appear to satisfy the condition $Q(0) < 1$ for all $d > 2$ with the second derivative of $|Q|$ positive at $\xi = 0$. In contrast, all of the branches bifurcating from $(0, \gamma_1)$ appear to satisfy $Q(0) > 1$ for all $d > 2$, with the second derivative of $|Q|$ negative at $\xi = 0$.

Each solution branch can be characterised by the number of bumps of the function $|Q(\xi)|$ when d is close to 2. We label each solution branch by the integers (m, n) such that $m = 0$ and 1 corresponds to a branch bifurcating from γ_0 and from γ_1, respectively, and n is the number of *maxima* of $|Q(\xi)|$ for $\xi \geq 0$ when d is close to 2. Thus the branch identified in [LPSS88b] has the label (1, 1). We conjecture that there is no upper limit to the maximum value of n possible.

3.2.1. Starting points on the branch. All branches were started from solutions obtained at $\mathbf{d} = \mathbf{2.01}$ and the values of (A, Γ) obtained using the shooting procedure with $X = 500$. The resulting values indexed according to the bifurcation point are shown in Tables 3.1 and 3.2.

A feature of these solutions visible from the tables is that as n increases the value of Γ is monotone increasing in the first table and monotone decreasing in the second. The value of A is monotone decreasing in both. Furthermore, the value of A corresponding to the curve $(0, n)$ lies between the two values of A corresponding to the curves $(1, n)$ and $(1, n + 1)$,

TABLE 3.2
Branches Bifurcating from the Ground State

Γ	A	(m, n)
2.120627439	0.385950653	(1, 1)
2.083537069	0.159401767	(1, 2)
2.054680304	0.108972064	(1, 3)
2.026406398	0.083476799	(1, 4)
1.998756776	0.067788407	(1, 5)
1.971847572	0.057096976	(1, 6)
1.827563573	0.029320039	(1, 12)

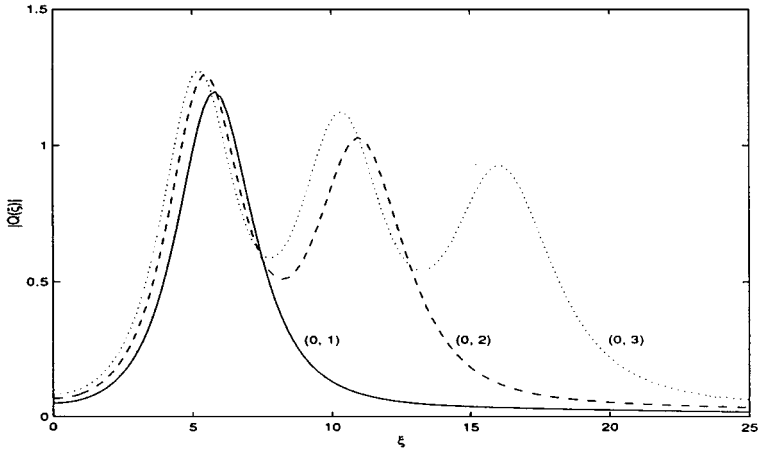

FIG. 3.2. The (0, 1), (0, 2), and (0, 3) solutions when $d = 2.01$.

and the value of A corresponding to the curve $(0, n)$ is approximately equal to the value corresponding to the curve $(1, n+1)$.

In Fig. 3.2 we plot the function $|Q(\xi)|$ for $0 \le \xi \le 25$ for the solutions labeled (0, 1), (0, 2), and (0, 3). The multi-bump nature of these solutions is very evident. Observe that all the maxima have similar magnitudes and locations.

In Fig. 3.3 we plot similarly the solutions labeled (1, 1), (1, 2), and (1, 3) together with the ground state solution $R(\xi)$. It is clear from this figure that the labeled solutions each start close to the ground state but that the solutions (1, 2) and (1, 3) have additional bumps. Note also that the second maxima of the solutions (1, 2) and (1, 3) are close to each other.

It is also interesting to compare the solutions (0, 1) and (1, 2), which exist for very similar values of A. These are plotted together in Fig. 3.4. Observe that although the behaviour of both for small ξ is quite different, the asymptotic behaviour as ξ increases is very similar, and in particular note the close correspondence of the bumps. A comparable phenomenon occurs for the solutions labeled (0, 2) and (1, 3).

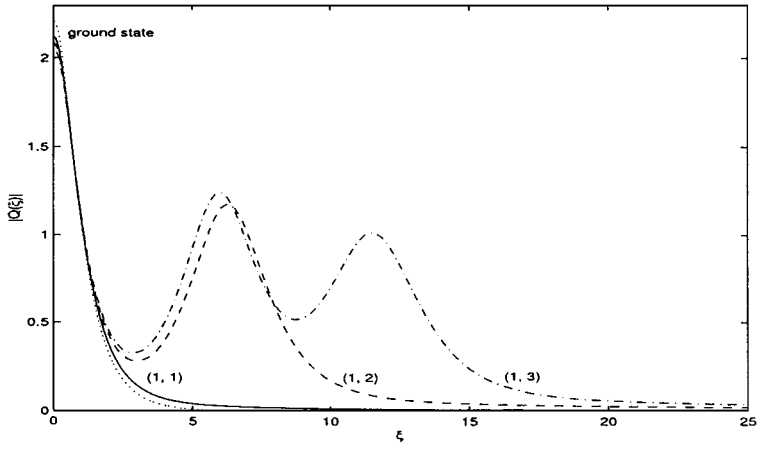

FIG. 3.3. The (1, 1), (1, 2), and (1, 3) solutions when $d = 2.01$.

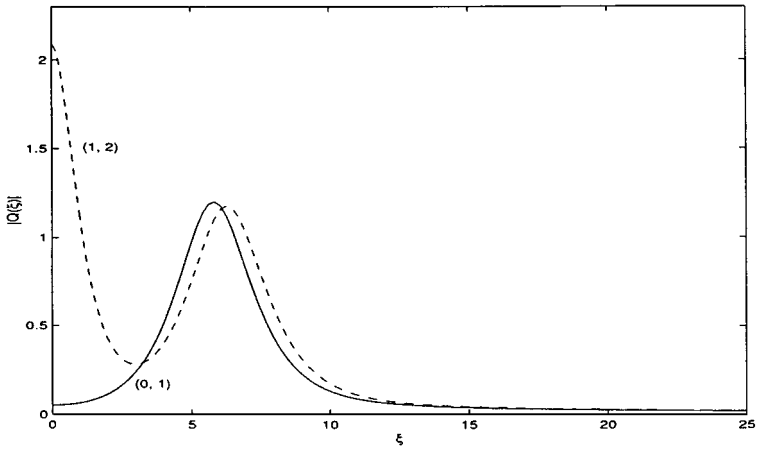

FIG. 3.4. A comparison of the (0, 1) and (1, 2) solutions when $d = 2.01$.

A different way to represent the solutions is to use the pseudo-phase-plane introduced in [KL95]. For this we define

$$C = |Q| \qquad \text{and} \qquad D = C_\xi / C = \mathrm{Re}(Q_\xi / Q).$$

In these coordinates a solution which varies slowly at infinity has

$$C \sim \alpha/\xi \qquad \text{and} \qquad D \sim -1/\xi \text{ as } \xi \to \infty.$$

Thus, this solution will approach the origin in the (C, D) plane along a straight line of gradient $-1/\alpha$. On the other hand, a solution which oscillates rapidly at infinity has

$$C \sim \alpha/\xi \qquad \text{and} \qquad D \sim \frac{a\beta}{\alpha}\xi^{3-d} 2a \cos(a\xi^2/2 + 2\log(\xi)/a),$$

so that D both oscillates rapidly and decays (or even grows) slowly. Thus, solutions in the (C, D) plane which obey the condition (2.22) are easy to distinguish from those which do not.

In Fig. 3.5 we plot the (C, D) phase plane of the first three solutions bifurcating from zero. This figure is directly comparable with Fig. 3.2. A similar picture for the solutions bifurcating from the ground state is presented in Fig. 3.6. The looping nature of the solutions is clear in these pictures.

3.2.2. Continuing the solutions for increasing d. As discussed earlier, each of the solutions described above serves as a starting point of a branch of solutions. In Figs. 3.7 and 3.8 we give two bifurcation diagrams for these solutions, plotting the values of A and of Γ over a range of values of d varying from $d = 2.000001$ to $d = 4$. The graph for the values of A show that A is a *monotone increasing* function of d, with $A \to 0$ as $d \to 2$. Note furthermore that the ordering of the values of A on each of the curves for $d = 2.01$ (such that the value of A on the curve $(0, n)$ lies between the values for $(1, n)$ and $(1, n + 1)$), continues for all values of d, and we conjecture that the curves do not intersect at any point. From Fig. 3.8 the division of the solutions into two groups is very evident, with $Q(0)$ tending either to 0

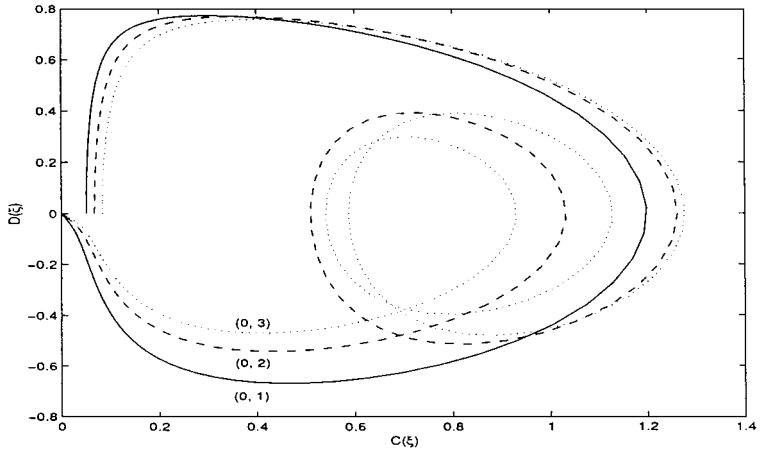

FIG. 3.5. The phase plane of the (0, 1), (0, 2), and (0, 3) solutions when $d = 2.01$.

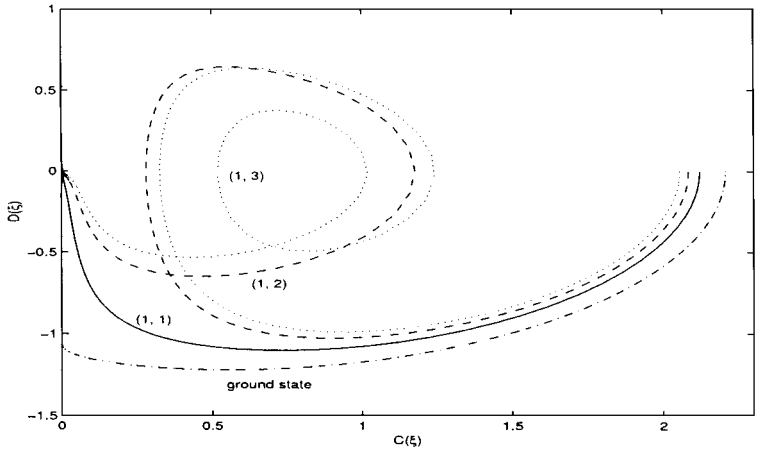

FIG. 3.6. The phase plane of the (1, 1), (1, 2), and (1, 3) solutions when $d = 2.01$.

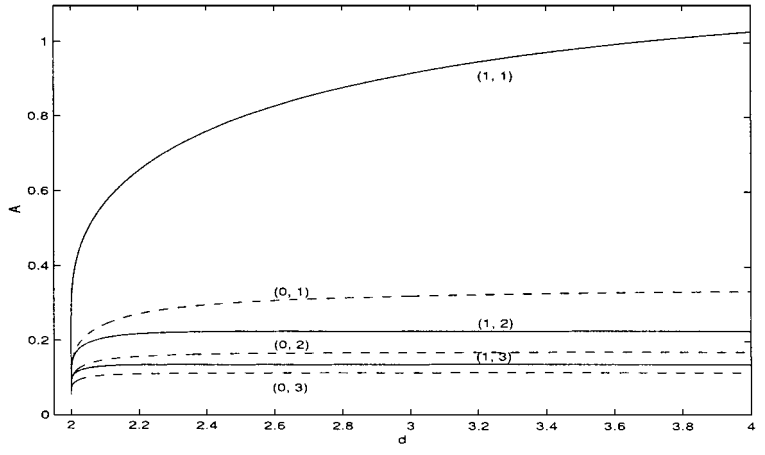

FIG. 3.7. The value of A as a function of d for each of the branches.

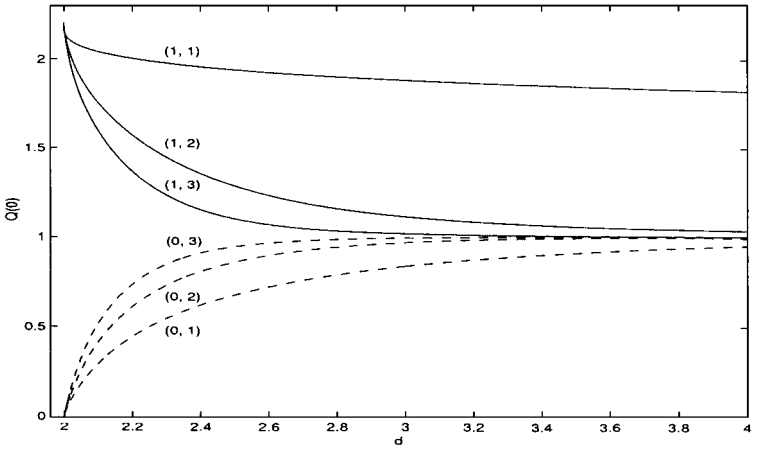

FIG. 3.8. The value of Γ as a function of d for each of the branches.

or to γ_1 as $d \to 2$. As $d \to 4$ (and presumably for larger values of d) we note that $Q(0) \to 1$. For the branches bifurcating from the zero solutions the curves approach $Q(0) = 1$ from below, and for the other branches they approach it from above.

The case of $d = 3$ is of physical interest. All of the curves continue to $d = 3$. The corresponding values of (A, Γ) are given in Table 3.3, divided into the two branches for clarity.

The resulting functions $|Q(\xi)|$ for the curves labeled (0, 1), (0, 2), (0, 3) are plotted in Fig. 3.9, and the corresponding curves in the (C, D) plane plotted in Fig. 3.10. Similar figures for the curves (1, 1), (1, 2), (1, 3) are given in Figs. 3.11 and 3.12. Observe that some of the loops present in these branches when $d = 2.01$ have opened out when $d = 3$.

3.2.3. Continuing the solutions as $d \to 2$. The limit as $d \to 2$ corresponds to the case studied in [KL95]. To investigate the behaviour in this case we consider three branches, namely (0, 1), (1, 1), and (1, 3) in the limit of d small.

Branch (1, 1). This corresponds precisely to the solution in [KL95] which is constructed as a perturbation of the ground state for $\xi < a^{-1/2}$ of the slowly varying solution when $\xi > a^{-3/2}$, with a matching between these two regimes obtained by comparing the solution with a parabolic cylinder function. Values of (A, Γ) for various values of d are given in Table 3.4.

In Fig. 3.13 we plot the resulting solutions $|Q(\xi)|$ together with the ground state solution and in Fig. 3.14 the same solutions in the (C, D) plane. The rapid convergence towards the ground state is clear.

TABLE 3.3

Γ	A	(m, n)
0.8399592743	0.3212400792	(0, 1)
0.9716454540	0.1697328431	(0, 2)
0.9982277883	0.1154776778	(0, 3)
1.8856569872	0.9173561430	(1, 1)
1.1166549497	0.2269653116	(1, 2)
1.0211870804	0.1377250206	(1, 3)

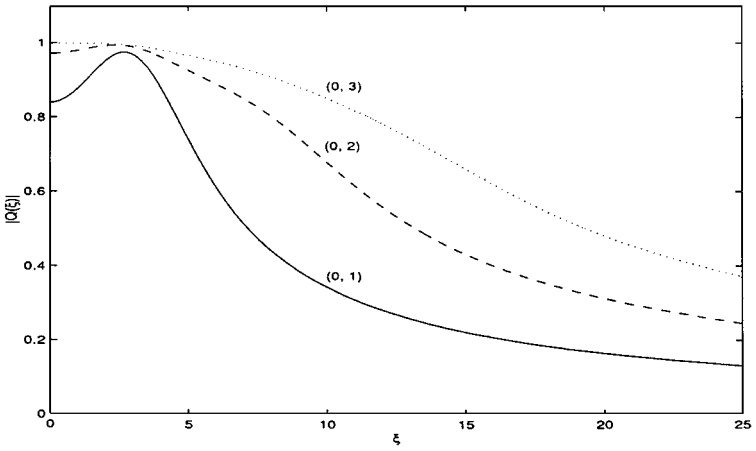

FIG. 3.9. The curves (0,1), (0, 2), and (0, 3) when $d = 3$.

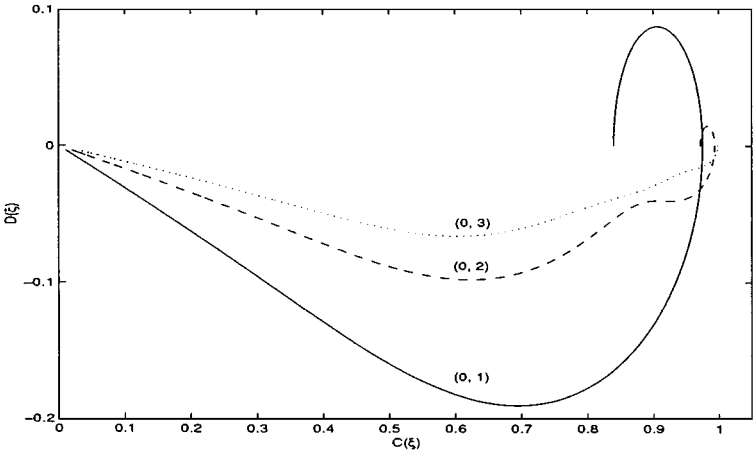

FIG. 3.10. The phase plane of the curves (0, 1), (0, 2), and (0, 3) when $d = 3$.

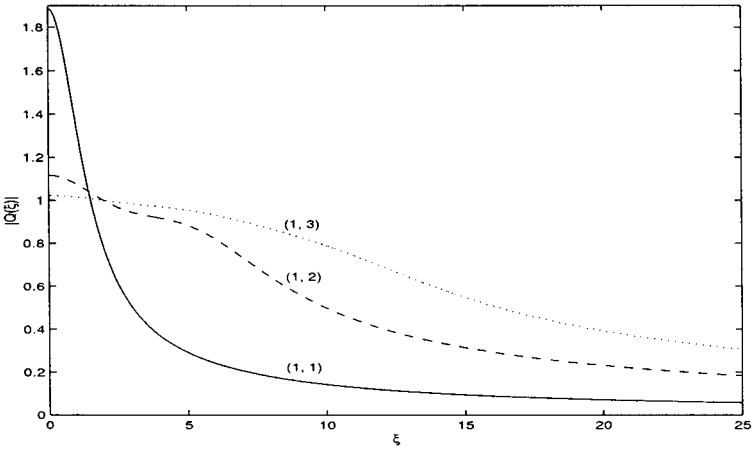

FIG. 3.11. The curves (1, 1), (1, 2), and (1, 3) when $d = 3$.

TABLE 3.4

d	Γ	A
2.01	2.120627441051382	0.3859506507555086
2.001	2.157338250885611	0.2932307852829842
2.0001	2.175013262845138	0.2374712003157395
2.000001	2.190154601923612	0.1730560597671120
2.00000001	2.196333944737588	0.1366120916995973
2.0000000001	2.199490232697582	0.1130409067693504

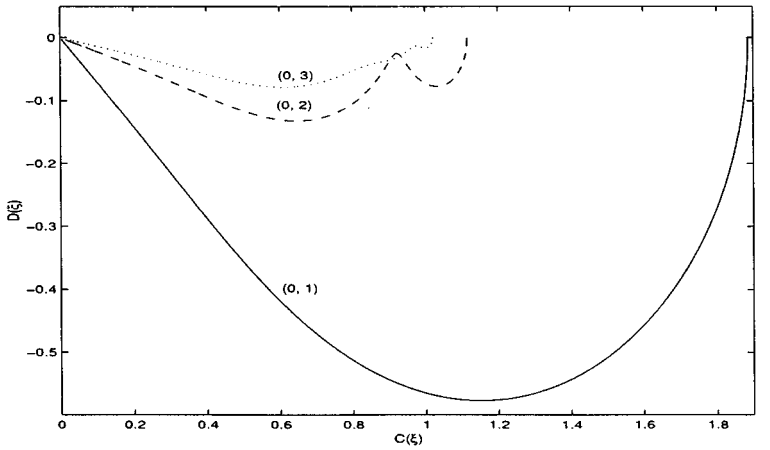

FIG. 3.12. The phase plane of the curves (1, 1), (1, 2), and (1, 3) when $d = 3$.

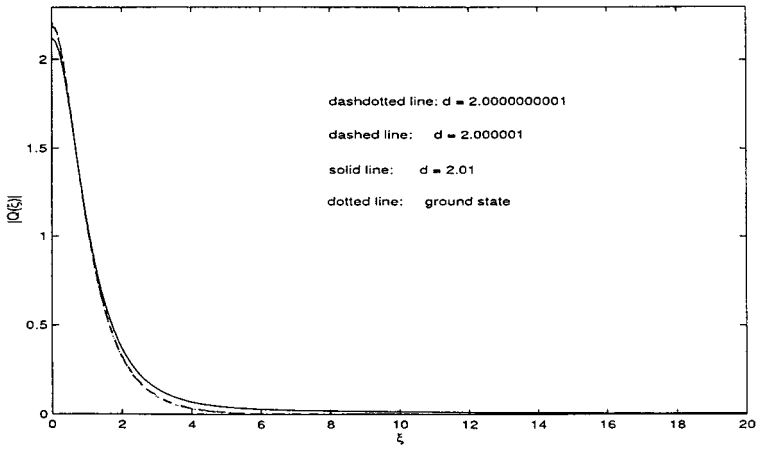

FIG. 3.13. The curve (1, 1) as $d \to 2$.

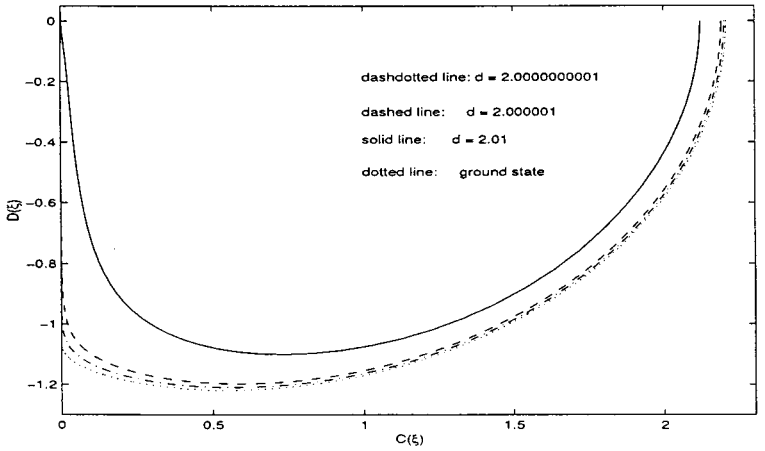

FIG. 3.14. The phase plane of the curve (1, 1) as $d \to 2$.

Branch (1, 3). For comparison, the values for a multi-bump solution which also bifurcates from the ground state are shown in Table 3.5.

In Fig. 3.15 we plot the resulting solutions $|Q(\xi)|$ again compared with the ground state. We observe that all three solutions are initially close to the ground state, with the region for which they are close increasing as d approaches 2. This is as predicted by [KL95] in which it is shown that $Q(\xi)$ is close to $R(\xi)$ for $\xi < 1/\sqrt{a}$ as $a \to 0$. Furthermore, all solutions decay for large values of a, again in accord with the predictions of [KL95] for $\xi > 1/a^{3/2}$. Where these solution differ from those considered by [KL95] is in the intermediate behaviour for which $|Q(\xi)|$ displays a multi-bump phenomenon. If we define $y = a\xi$, a plot of $|Q|$ as a function of y is given in Fig. 3.16. In this we can see that the locations in y of the maxima and minima of $|Q(y)|$ are approximately constant, implying that the multi-bumped behaviour occurs when $\xi = \mathcal{O}(1/a)$ which is between $1/\sqrt{a}$ and $1/a^{3/2}$. Note further, however, that in the ξ coordinate, the bumps appear to be translates of each other. A graph of these three solutions in the (C, D) plane is given in Fig. 3.17.

Branch (0, 1). Finally, the (Γ, A) values for the first branch bifurcating from the zero solution are given in Table 3.6.

In Fig. 3.18 we plot the solutions for these values and see a similar phenomenon to that in the above calculation, viz., that the solutions all look similar, with the bumps appearing to be invariant apart from a translation as d is reduced. Plotting the solutions against $y = a\xi$,

TABLE 3.5

d	Γ	A
2.01	2.054680413660254	0.108972053473581
2.001	2.178637993258769	0.088084243354237
2.0001	2.200151746863060	0.073266114342636
2.00001	2.203694245603700	0.062877129274365
2.000001	2.204551856643807	0.055232787596050

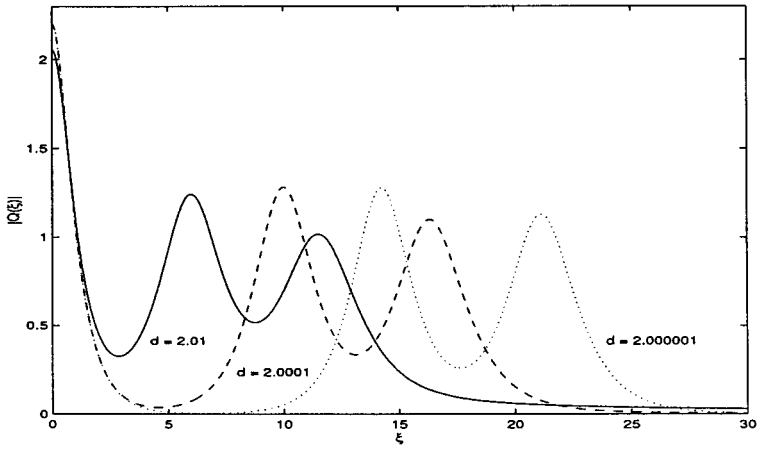

FIG. 3.15. The curve (1, 3) as $d \to 2$.

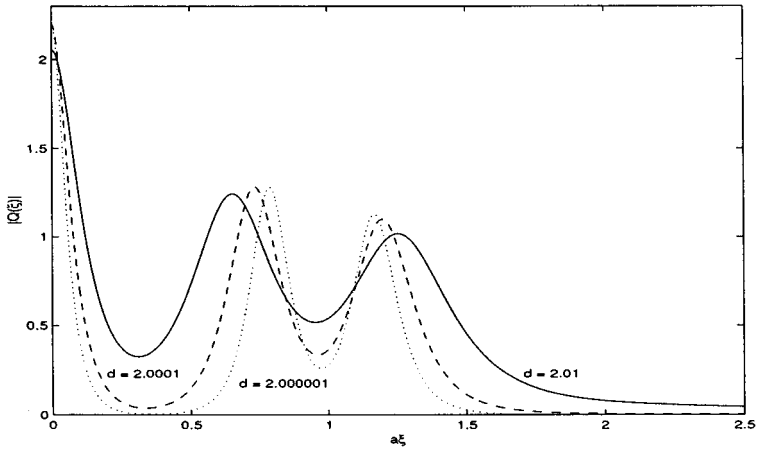

FIG. 3.16. A rescaling of the curve (1, 3) as $d \to 2$.

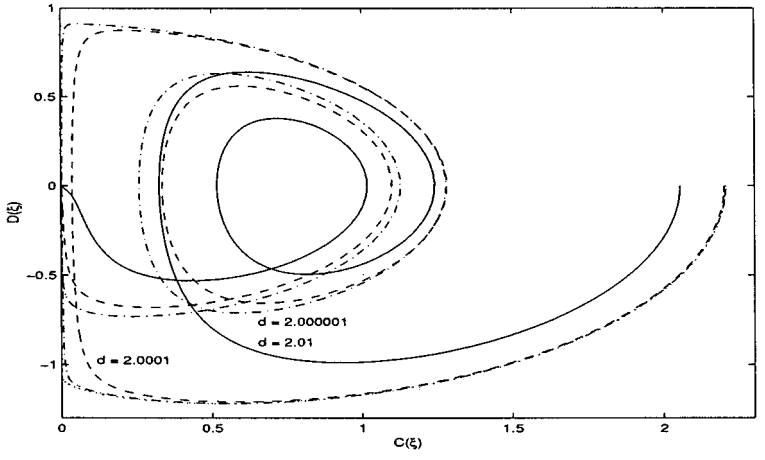

FIG. 3.17. The phase plane of the curve (1, 3) as $d \to 2$.

TABLE 3.6

d	Γ	A
2.01	0.050957837350847	0.166124963113730
2.001	0.007482754125859	0.123033038440185
2.0001	0.001121615461758	0.097998891850343
2.00001	0.000172826027901	0.081700091451878
2.000001	0.000027092964890	0.070188665579905

we see very clearly that the location of the maximum point is almost invariant in this rescaled variable, again implying that the multi-bumped behaviour occurs for $\xi = \mathcal{O}(1/a)$ (see Fig. 3.19). A graph in the (C, D) plane is given in Fig. 3.20.

3.2.4. Scalings as $d \to 2$. We find from Fig. 3.7 that on all the branches A decreases extremely fast as $d \to 2$. LeMesurier *et al.* [LPSS88b] and Kopell and Landman [KL95] used asymptotic arguments to imply that on the branch (1, 1)

$$d(a) - 2 \approx \frac{k}{a} \exp^{-\lambda/a} \qquad \text{as } a \to 0, \tag{3.7}$$

where $k \approx 12.75$ could be computed analytically and $\lambda = \pi$. It appears from our calculations that similar behaviour occurs for the other branches (although the calculation of k is very sensitive). Using a least squares fit to calculate k and λ gives the results shown in Table 3.7.

In contrast, a rather different scaling law is observed for $Q(0)$. In particular, on the branches labeled $(0, n)$ we find that there are exponents γ_n and constants k_n for which

$$Q(0) = k_n(d-2)^{\gamma_n}.$$

The resulting values of these are shown in Table 3.8.

An explanation of this scaling phenomenon together with an asymptotic description of the multi-bump solutions will be given in a forthcoming paper.

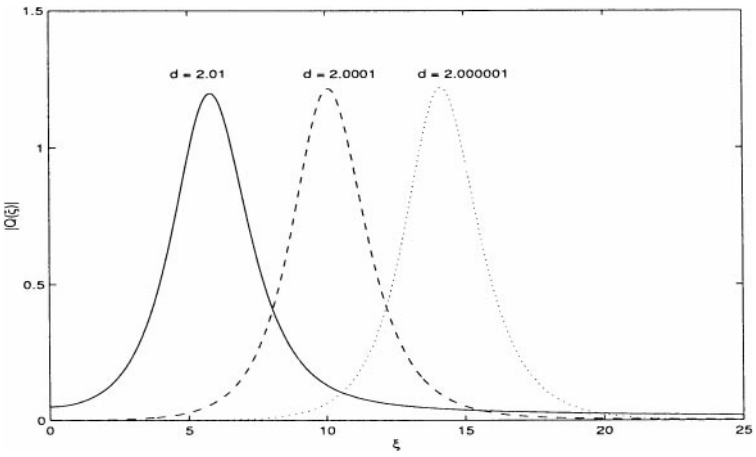

FIG. 3.18. The curve (0, 1) as $d \to 2$.

TABLE 3.7

(m, n)	λ	k	(m, n)	λ	k
(1, 1)	3.1412	13.23	(0, 1)	1.2234	2.61
(1, 2)	1.2217	2.45	(0, 2)	1.1019	26.10
(1, 3)	1.1115	30.32	(0, 3)	0.9853	96.32

TABLE 3.8

n	γ_n	k_n
1	0.8018	1.753
2	0.8669	3.248
3	0.9191	5.213

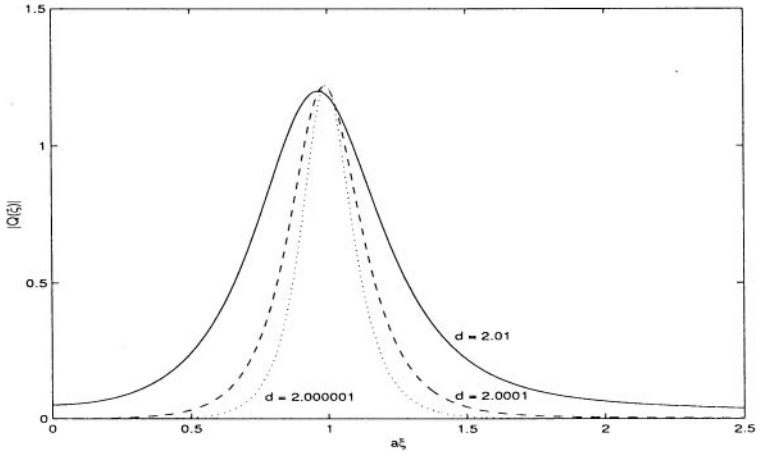

FIG. 3.19. The rescaled curve (0, 1) as $d \to 2$.

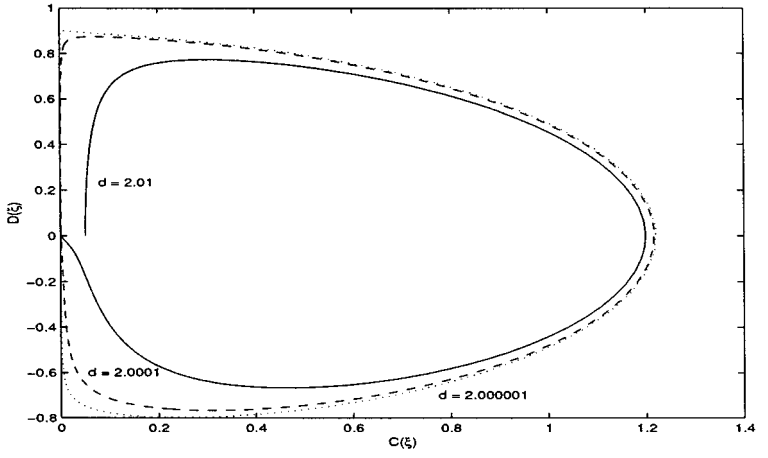

FIG. 3.20. The phase plane of the curve (0, 1) as $d \to 2$.

4. A NUMERICAL ALGORITHM BASED UPON INVARIANT METHODS

The functions calculated in the previous section are all possible candidates for the evolution of the solutions of the nonlinear Schrödinger equation, but the analysis gives no indication as to their stability or indeed the evolution of the solutions of NLS from arbitrary initial data. To investigate such a form of blow-up behaviour requires the use of a sophisticated numerical approach. In this section we describe and analyse such as numerical method for solving the time dependent problem (1.1), and in the next section we use this method to investigate the stability of the self-similar solutions calculated above. The method we describe exploits the symmetries of the NLS and has close similarities to the dynamic rescaling methods developed by Papanicolaou *et al*. but is rather easier to implement and has applicability to a wide range of problems. Our formulation is based upon the scaling invariant moving mesh methods described in [BHR96, BCHR96, BC98] which have proved very effective for solving a variety of problems involving blow-up in systems of partial differential equations which exhibit an invariance under rescaling. These methods involve a method of lines discretisation of $u(r,t)$ on a moving mesh $R_i(t)$ determined by using a relaxed form of equidistribution. The methods are so constructed that any natural scale invariance in the original problem is automatically inherited by the numerical solution, and yet they allow a natural incorporation of general initial and boundary values.

4.1. *Semi-discrete Approximations*

To construct the approximation method we introduce a discrete approximation $U_i(t)$ to $u(r,t)$ at the point, $R_i(t)$. The number N of mesh-points $R_i(t)$ is fixed throughout the computation, but the location of each point changes to allow for a finer mesh close to the singularity.

To approximate the radially symmetric solutions of the partial differential equation (1.1) we use a Lagrangian formulation of it in conservation form, viz.,

$$ir^{d-1}\left[\frac{du}{dt}-\frac{\partial u}{\partial r}\frac{dr}{dt}\right]+\left(r^{d-1}u_r\right)_r+r^{d-1}u|u|^2=0, \tag{4.1}$$

with boundary conditions

$$u_r(0,t)=0, \qquad u(L,t)=0. \tag{4.2}$$

The latter boundary condition is an approximation to the boundary condition on u at infinity, and L is taken suitably large and fixed.

Equation (4.1) is discretised in space on the mesh $R_i(t)$ by representing the approximation to $u(r,t)$ as a piecewise cubic polynomial, using Hermite cubic shape functions on each interval $[R_i, R_{i+1}]$. Taking collocation at suitable Gauss points within the intervals and enforcing the exact solution of Eq. (4.1) at these points, we obtain a set of N differential equations for U_i and R_i of the form

$$A(U_i, R_i)\frac{dU_i}{dt}+B(U_i, R_i)\frac{dR_i}{dt}+F(U_i, R_i)=0, \tag{4.3}$$

where A, B, and F are appropriate nonlinear functions of U_i and R_i. Details of this procedure are given in [HR96].

The mesh $R_i(t)$ is determined by equidistribution using a relaxed form of the procedure described in [DD87]. Supposing that $R_0(t) \equiv 0$ and $R_N(t) \equiv L$, the mesh points $R_i(t)$ are chosen to equidistribute a monitor function of the solution $M(u, u_r) > 0$. In [DD87] it is proposed that R_i satisfy the integral condition

$$\int_0^{R_i} M dr = \frac{i}{N} \int_0^L M\, dr; \qquad i = 0, \ldots, N. \tag{4.4}$$

A mesh satisfying (4.4) will be said to be *equidistributed*. This formulation has two disadvantages for our purpose. First, it requires a carefully selected mesh at time $t = 0$. Second, it is prone to mesh instability [HR97]. Instead we consider a relaxed form of (4.4) (called MMPDE6 in [HRR94a, HRR94b]) and require that $R_i(t)$ satisfies the stiff integro-differential equation

$$\tau \dot{R}_i = -\left(\int_{R_0}^{R_i} M\, dr - \frac{i}{N} \int_0^L M\, dr \right), \qquad i = 0, \ldots, N. \tag{4.5}$$

It is convenient for the derivation and analysis of this method to consider $R_i(t)$ as discrete values of a continuous mesh function $R(\xi, t)$ so that $R_i \equiv R(\frac{i}{N}, t)$. Here ξ is a "computational" coordinate in the fixed interval [0, 1]. Differentiating (4.5) twice with respect to ξ gives [HRR94a]

$$\tau R_{t\xi\xi} = -(M R_\xi)_\xi. \tag{4.6}$$

For a given function M, Eq. (4.6) can be discretised using a simple three-point finite difference with equally spaced values of ξ. This yields a set of ordinary differential equations for $R_i(t)$ of the form

$$\tau C \dot{R}_i = D(R_i, U_i), \tag{4.7}$$

where D depends on R_i, U_i through the monitor function M. An elementary but very revealing calculation gives the natural time scale for the evolution of the mesh under the action of this differential equation. Suppose that Δ is the "relaxation-time" under which macroscopic changes of the mesh occur. Then by considering the dimensions of similar quantities in (4.6) we have that

$$\Delta \sim \frac{\tau}{M}. \tag{4.8}$$

If τ is small and M is large, the mesh evolves rapidly. This result is crucial in our subsequent analysis of the performance of the method.

To implement the method, the two systems of Eqs. (4.3) and (4.7) are solved simultaneously using a BDF method (in particular the stiff integration package DDASSL [Pet82]). We observe that this method is convenient to use, and while it does not generally inherit the symplectic structure of the time-evolution of the PDE, it is unlikely that the discrete Eqs. (4.3) and (4.7) are themselves Hamiltonian, thus somewhat reducing in advance the effectiveness of using a Hamiltonian integrator. To maintain the accuracy of the temporal integration we use high relative and absolute tolerances in the ODE integration package and constantly monitor the error estimates throughout the integration procedure.

4.2. *Invariant Meshes*

Both the PDE (1.1) and its transformed form (4.1) are invariant under translations in time, space, and the scaling transformations in (2.5) and (2.6). All of these transformations are important in the resulting dynamics of the solution, and it is thus highly desirable that this invariance is reflected in the numerical scheme. We argue that as the scaling invariance dominates the formation of the singularity, a scaling invariant numerical scheme will also resolve the singularity effectively. To achieve this invariance we insist that if $(U_i(t), R_i(t))$ is a solution of the discrete equations then so should be the rescaled solution $(\lambda^{-1/2}U_i(\lambda t), \lambda^{1/2}R_i(\lambda t))$, provided that we exclude the boundary condition at R_N. A simple calculation shows that the differential equation (4.3), which is derived directly from the PDEs, automatically inherits all the required scaling properties. However, to have a solution of (4.5) which is also invariant requires a careful choice of the monitor function M. Under the scaling transformation, (4.5) becomes

$$\lambda^{-1}\dot{R}_{\xi\xi} = \left[M\left(\lambda^{-\frac{1}{2}}u, \lambda^{-1}u_r\right)R_\xi\right]_\xi,$$

and hence to obtain scaling invariance we require that $M(u, u_r)$ satisfy

$$\lambda M\left(\lambda^{-\frac{1}{2}}u, \lambda^{-1}u_r\right) = M(u, u_r). \tag{4.9}$$

The simplest monitor function satisfying (4.9) is

$$M(u, u_r) \equiv |u|^2. \tag{4.10}$$

A more subtle monitor function which gives better resolution of a varying curve but has similar invariance is

$$M(u, u_r) = \sqrt{\alpha|u|^4 + \beta|u_r|^2}. \tag{4.11}$$

We use both (4.10) and (4.11). Observe that M is large when u and u_r are large. Consequently, more mesh points will be placed near singularities. The system (4.3) and (4.7) with M given by (4.10) or (4.11) describes a dynamical system which, apart from the right boundary condition, is scaling invariant. Such a system admits numerical self-similar solutions, mimicking the analytic solutions of the previous section. In particular, the numerical scheme admits solutions of the form

$$U_i(t) = (2a(T-t))^{-\frac{1}{2}}\exp\left(-\frac{i}{2a}\log(T-t)\right)Q_i, \qquad R_i(t) = (2a(T-t))^{\frac{1}{2}}Y_i, \tag{4.12}$$

where Q_i and Y_i are independent of time. The function Q_i is automatically a discretisation using collocation of the continuous function $Q(y)$ on the non-uniform mesh Y_i. The numerical scheme automatically preserves self-similar structure when it exists and finds the correct coordinate transformation in such a case. However, it is important to note that we do not impose a self-similar (or indeed any other) structure upon the solution, and the numerical method can start from arbitrary initial data. A desirable (but very difficult to prove) property of the scheme is that the stability properties of any self-similar solution should be inherited. We have observed this numerically in all of our experiments (cf. Section 5).

When implementing the numerical method it is found that using the system (4.7) can lead to instabilities. This is because, with a fixed number of mesh points, too many points are placed in a neighbourhood of the singularity and too few are placed near the boundary points. To prevent this, a smoothing of the monitor function is used so that if M_i is the value of M at the point R_i then we replace M_i in the finite difference discretisation of (4.7) by

$$\tilde{M}_i = \sqrt{\left[\sum_{k=i-ip}^{i+ip} (M_k)^2 \left(\frac{2}{3}\right)^{|k-i|}\right] \Bigg/ \left[\sum_{k=i-ip}^{i+ip} \left(\frac{2}{3}\right)^{|k-i|}\right]}, \tag{4.13}$$

where ip is a user-defined, smoothing parameter.

The effect (4.13) is to preserve the symmetry invariance close to the point of singularity but to gradually weaken it nearer the boundary.

4.3. *Analysis of the Scheme*

We now briefly analyse the performance of the resulting schemes when $d > 2$ by considering how well they capture the behaviour of a singularity evolving in the self-similar manner. At a time t close to the blow-up time T, the solution undergoes macroscopic changes in a time-scale of order $(T-t)$. In comparison, the relaxation time for the mesh is $\Delta = \tau/M$. If $M = |u|^2$ then this gives

$$\Delta = \tau/|u|^2 = \tau L^2 = \tau(T-t),$$

with an exactly similar result for $M = \sqrt{\alpha|u|^4 + \beta|u_r|^2}$. If τ is small, the mesh relaxes on a time scale which is small compared to the natural problem time scale, but it scales in the same way as the original solution, giving it excellent stability properties. As a result the mesh converges rapidly to, and stays on, the equilibrium manifold. On this manifold we have from (4.4) that

$$\int_0^{R_i} M\, dr = \frac{i}{N} \int_0^L M\, dr,$$

so that if $M = |u|^2$

$$\int_0^{R_i} \frac{1}{2a(T-t)} \left| Q\left(\frac{r}{2a(T-t)}\right)\right|^2 dr = \frac{i}{N} \int_0^L \frac{1}{2a(T-t)} \left| Q\left(\frac{r}{2a(T-)}\right)\right|^2 dr.$$

Thus

$$\begin{aligned} \int_0^{R_i/(2a(T-t))^{1/2}} |Q(y)|^2\, dy &= \frac{i}{N} \int_0^{L/(2a(T-t))^{1/2}} |Q(y)|^2\, dr \\ &\approx \frac{i}{N} \int_0^{\infty} |Q(y)|^2\, dy \qquad \text{as } t \to T. \end{aligned} \tag{4.14}$$

Defining the function $J(z)$ by

$$J(z) = \int_0^z |Q(y)|^2\, dy, \tag{4.15}$$

we have

$$R_i = (2a(T-t))^{1/2} J^{-1}\left(\frac{i}{N} J(\infty)\right) \equiv (2a(T-t))^{1/2} Y_i. \tag{4.16}$$

The formula (4.16) then gives the mesh for values of i for which i/N is not close to one. Indeed, if i/N is small then

$$R_i \approx (2a(T-t))^{1/2} \frac{i}{N} \frac{J(\infty)}{|Q(0)|^2}, \tag{4.17}$$

so that R_i scales exactly as the transformed coordinate of the self-similar solution, with the mesh points distributed uniformly within the evolving singularity.

In contrast, as $i \to N$ we have that $Y_i \to \infty$, and a more careful calculation using the approximation $|Q(y)| \sim \alpha/y$ gives

$$\frac{1}{R_i} \sim \frac{1}{L} - \left(1 - \frac{i}{N}\right)\left(\frac{J_\infty}{\alpha(2a(T-t))^{1/2}} - \frac{1}{L}\right), \tag{4.18}$$

and hence as $i \to N$

$$U_i \sim \frac{1}{(2a(T-t))^{1/2}} \frac{\alpha}{L} - \left(1 - \frac{i}{N}\right)\left(\frac{J_\infty}{(2a(T-t))^{1/2}} - \frac{\alpha}{L}\right). \tag{4.19}$$

In practice, however, the effects of smoothing and of the truncated boundary condition act to distort the formulae (4.18) and (4.19) if i is very close to N.

5. NUMERICAL COMPUTATIONS OF TIME DEPENDENT SOLUTIONS

In this section, we use the moving collocation method mentioned above to solve (1.1) in three dimensions with a variety of initial conditions. Our purpose is to investigate the stability of the self-similar solutions computed in the previous sections. In particular, we consider taking both monotone and non-monotone initial data.

5.1. *Monotone Initial Conditions*

For our initial calculation we take $L = 5$ and

$$u(r,0) = \begin{cases} 6\sqrt{2}e^{-r^2}, & \text{if } 0 \le r \le 5, \\ 0, & \text{if } r > 5. \end{cases} \tag{5.1}$$

This problem has been considered by many authors (see [MPSS86, TS92, ADKM92]). McLaughlin *et al.* [MPSS86] computed $T \approx 0.034301966$. Furthermore, Akrivis *et al.* [ADKM92] by using a refined Galerkin-finite element method demonstrated that the blow-up behaviour was indeed self-similar.

To apply the method described in the previous section we choose the monitor function to be

$$M(r,t) = \sqrt{|u(r,t)|^4 + 2|u_r(r,t)|^2}, \tag{5.2}$$

take $\tau = 10^{-6}$, use a spatial smoothing parameter $ip = 5$, and set $N = 81$. Since the error tolerance for the time integration is sensitive for problems with singularities, it must be

TABLE 5.1

N	Monitor function	*atol*	Blow-up time
81	$\sqrt{2\|u_r\|^2 + \|u\|^4}$	$10^{-9} \nearrow 10^{-6}$	0.0343013614238
91	$\|u\|^2$	$10^{-9} \nearrow 10^{-5}$	0.0343013710865
61	$\|u\|^2$	$10^{-9} \nearrow 10^{-5}$	0.0343013774962

chosen carefully. While a small error tolerance gives more accurate solutions, if the tolerance is too small the CPU time can become excessive and cause breakdown earlier than desired near blow-up. Here we choose the relative tolerance to be $rtol = 10^{-9}$ and the absolute tolerance to change according to the maximum value of $|u|$, viz.,

$$\begin{aligned}
&\text{atol} = 10^{-9} && \text{if } |u(0,t)| \le 1000,\\
&\text{atol} = 10^{-8} && \text{if } 1000 < |u(0,t)| \le 30{,}000,\\
&\text{atol} = 10^{-7} && \text{if } 30{,}000 < |u(0,t)| \le 150{,}000,\\
&\text{atol} = 10^{-6} && \text{if } 150{,}000 < |u(0,t)|.
\end{aligned}$$

Using these parameters, we can reach a maximum computed value of $|u(0,t)| = 920{,}000$ for $t = 0.0343013614215$. To obtain the blow-up time, we use a nonlinear least squares fit by evaluating $u(0,t_j)$ at a series of times t_j and then consider the problem

$$\text{minimize} \sum_{j=1}^{m} [\log(A/\sqrt{T-t_j}) - \log(|u(0,t_j)|)]^2. \tag{5.3}$$

Here m corresponds to the time spread of the numerical computation, and its value is 2960 for which $|u(0,t_j)|$ varies from 6800 to 920,000. The best least squares fit is given by $A = 1.3918$ and $T = 0.03430136142381$, implying that $|u(0,t)| \sim 1.3918/\sqrt{T-t}$ (notice that the self-similar solution $|u(0,t)| = Q(0)/\sqrt{2a(T-t)} \approx 1.3921258/\sqrt{T-t}$ in (2.7)).

The numerical computations indicate that both the blow-up time T and the phase shift θ are relatively insensitive to the number of mesh points and the precise monitor function. In Table 5.1 we demonstrate this by calculating T for three sets of parameters.

In Fig. 5.1 we illustrate the development of the singularity by plotting $u(r,t)$ for several values of $t \to T$.

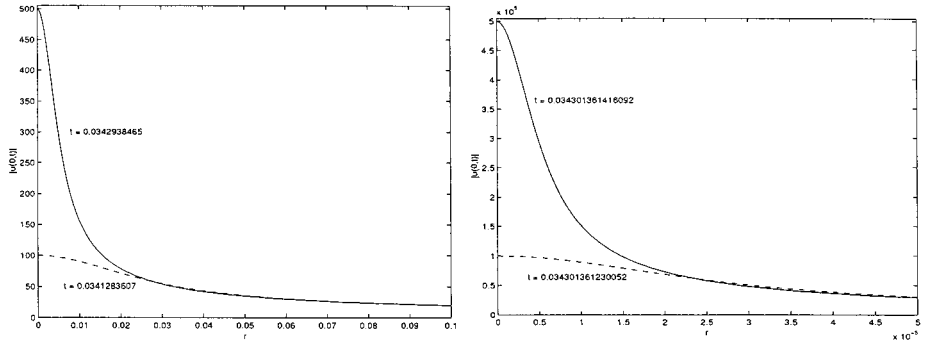

FIG. 5.1. Development of the singularity when $|u(0,t)| = 100$, 500, 100,000, and 500,000.

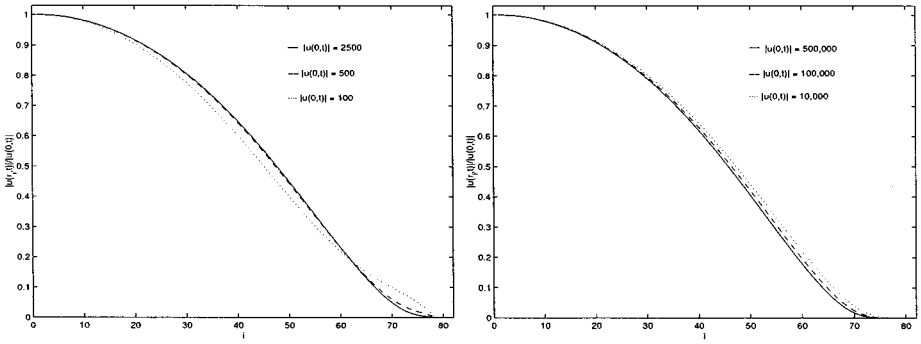

FIG. 5.2. $|u(x_i, t)|/|u(0, t)|$ versus i when $|u(0, t)| = 100$, 500, 2500, 10,000, 100,000, and 500,000.

In Fig. 5.2, we plot $|u(R_i, t)|/|u(0, t)|$ as a function of the node index i, for $|u(0, t)| = 100$, 500, 2500, 10,000, 100,000, and 500,000. These curves are almost invariant as $|u(0, t)|$ increases. This is precisely what would be expected of a self-similar solution and strongly implies that the numerical method has automatically identified the correct scaling properties of the solution.

In Fig. 5.3, we plot $R_i|u(0, t)|$ against $|\log(T - t)|$ for $i = 2, \ldots, 13$. From (4.16) it follows that for a solution evolving in a self-similar manner we should have

$$R_i|u(0, t)| \sim Y_i|Q_i| \qquad \text{which is independent of } t \text{ for large values of } |u(0, t)|.$$

This behaviour is confirmed by the figure, and we see further that the mesh points are distributed locally uniformly as predicted by (4.17).

We now compare the computed solution with the exact self-similar solution (2.7) derived from the solution of (2.8) on the branch (1, 1) in the case $d = 3$. To do this we look at solutions both starting from the Gaussian initial function and also from the two further initial functions

$$u(r, 0) = \begin{cases} 6\sqrt{2}/(1 + r^2), & \text{if } 0 \le r \le 200, \\ 0, & \text{if } r > 200, \end{cases} \tag{5.4}$$

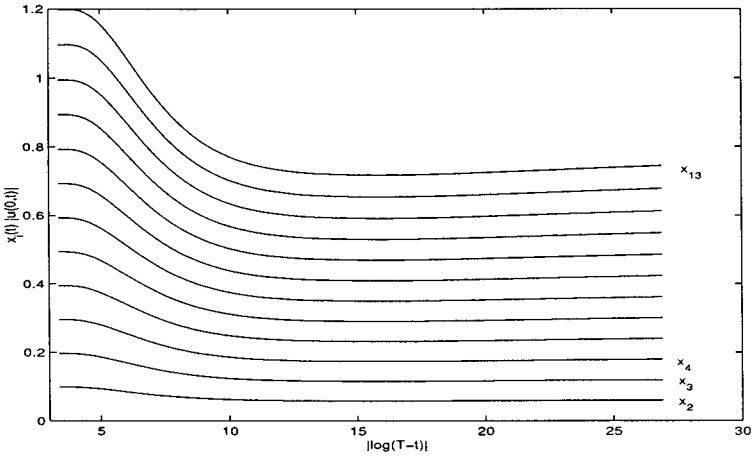

FIG. 5.3. $R_i|u(0, t)|$ versus $|\log(T - t)|$.

TABLE 5.2

Initial value	Line	N	Monitor function	*atol*	Blow-up time
(5.1)	Solid line	81	$\sqrt{2\|u_r\|^2+\|u\|^4}$	$10^{-9}\nearrow 10^{-6}$	0.03430136142
(5.4)	Dotted line	141	$(1+r)\sqrt{2\|u_r\|^2+\|u\|^4}$	$10^{-5}\searrow 10^{-7}$	0.03561777658
(5.5)	Dashed line	81	$\sqrt{2\|u_r\|^2+\|u\|^4}$	$10^{-9}\nearrow 10^{-5}$	0.08971350508

and

$$u(r,0)=\begin{cases}6/(1+r^2)^4, & \text{if } 0\le r\le 10,\\ 0, & \text{if } r>10.\end{cases} \tag{5.5}$$

The first, (5.4), is called the Lorentzian initial condition. Since the initial value $6\sqrt{2}/(1+r^2)$ approaches 0 relatively slowly as $r\to\infty$, we must use the large computational domain [0, 200]. We choose the monitor function to be $M=(1+r)\sqrt{|u|^4+2|u_r|^2}$ so that the mesh points are distributed more uniformly for $r>1$ compared with those generated by $M=\sqrt{|u|^4+2|u_r|^2}$, but so that scaling invariance is still retained for small r. The blow-up times estimated by using the least squares method for these initial functions are given in Table 5.2.

Here, *atol* is the absolute tolerance. The blow-up time is estiamted using the least squares fit procedure described above.

According to (2.7) the phase ϕ of $u(0,t)$ is given asymptotically by

$$\phi=\theta+\frac{1}{2a}\log(T/(T-t)),$$

so ϕ is asymptotically a linear function of $\tau\equiv-\log(T-t)$ with gradient $1/2a$. Figure 5.4 shows the three curves of ϕ for the three initial functions. Asymptotically these are all straight lines with almost identical slopes of approximately 0.5450 giving a $a\approx 0.9173$, which is precisely the value determined earlier.

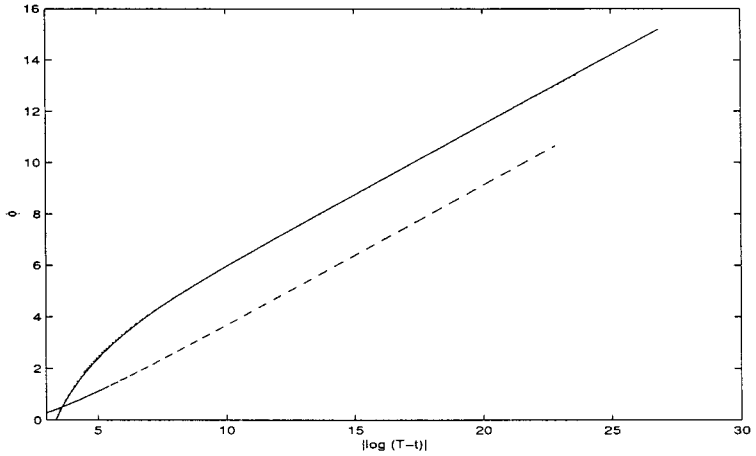

FIG. 5.4. The phase ϕ versus $|\log(T-t)|$ for the three curves (see Table 5.2 for the initial conditions and the corresponding lines).

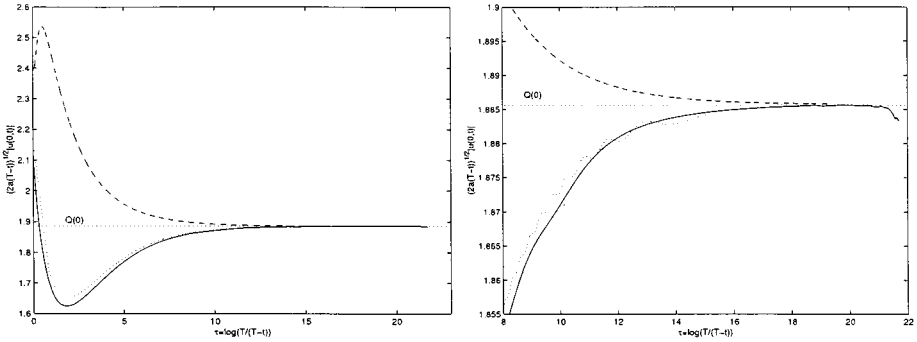

FIG. 5.5. $\sqrt{2a(T-t)}|u(0,t)|$ versus $\tau = \log(T/(T-t))$ with three different initial values (see Table 5.2). The vertical direction is enlarged near $Q(0)$ on the right.

In Fig. 5.5 we see the convergence of the rescaled function $\sqrt{2a(T-t)}|u(0,t)|$ plotted against $\tau = \log(T/(T-t))$ using the value of a estimated above. All three curves approach 1.88566, which implies that the amplitudes of all three solutions at the origin asymptotically approach the corresponding values of the exact self-similar solution (2.7) as $t \to T$, confirming the stability of this function. Observe that the three initial functions lead to similar decay rates, implying that the rate of asymptotic convergence toward the self-similar solution does not depend upon the initial data—rather on the local linearisation about the self-similar solution of the NLS in the rescaled variables. From a careful analysis of the figures it appears as though the decay rate is $\mathcal{O}((T-t)^{1/2})$ so that we conjecture that in the limit

$$u(0,t) = \frac{Q(0)}{\sqrt{2a(T-t)}} + C + \mathcal{O}((T-t)^{1/2}),$$

where the value of the constant C probably depends upon the initial conditions.

The global stability of the (1, 1) branch of self-similar solutions persists as d is reduced to 2. To see this, we choose the initial value (5.1) and take $d = 2.5$, 2.01, and 2.001. The corresponding rescaled solutions are plotted in Fig. 5.6, where we can see that the curves

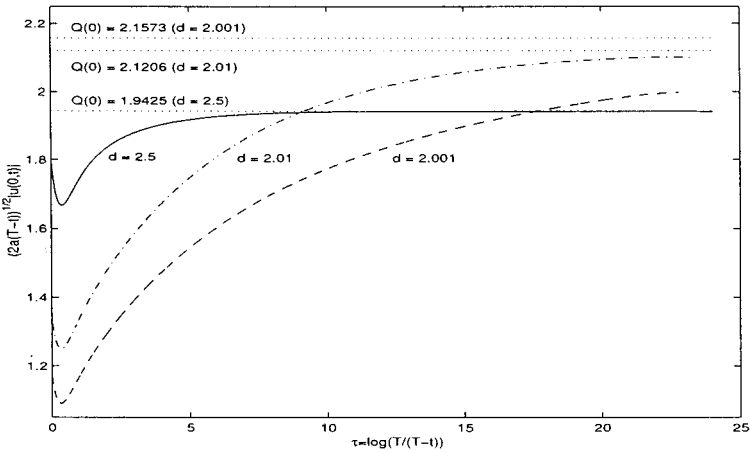

FIG. 5.6. $\sqrt{2a(T-t)}|u(0,t)|$ versus $\log(T/T-t)$ for $d = 2.5$ (solid line), $d = 2.01$ (dash-dotted line), and $d = 2.001$ (dashed line).

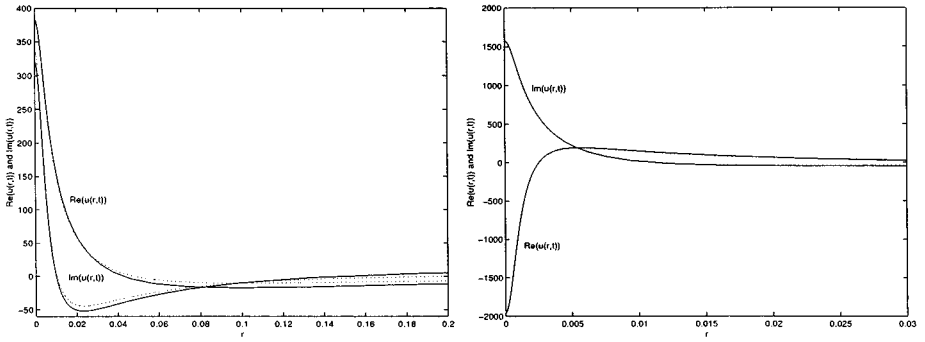

FIG. 5.7. $\mathrm{Re}(u(r,t))$ and $\mathrm{Im}(u(r,t))$ versus r for $t = 0.03429384648$ ($|u(0,t)| = 500$) on the left and $t = 0.03430106161$ ($|u(0,t)| = 2500$) on the right.

approach the corresponding values of $Q(0)$ as $t \to T$ with the rate of convergence slowing down markedly as $d \to 2$.

Taking the initial function (5.1), we now compare the solution curves as functions of r with the exact self-similar solution at three values of $t < T$ for which $|u|$ takes the respective values 500, 2500, and 100,000. In each case the phase θ of the self-similar solution (2.7) is chosen in such a way that the exact solution and the numerical solution have the same phase at the origin.

The real and imaginary parts of the numerical solution and the self-similar solution are given in Figs. 5.7 and 5.8 for three different times by using the initial values (5.1). Solid lines represent the numerical solutions and dotted lines represent the exact solutions (2.7). From the above figures, we can see that the corresponding curves converge as $t \to T$.

5.2. *Non-monotone Initial Data*

We now look at the effects of taking non-monotone initial data. The purpose of this calculation is to examine the stability of the self-similar solutions calculated in Section 3. To do this calculation we define an a priori blow-up time of $T = 0.1$ and take $\theta = 0$. Substituting these values into (2.7) with $t = 0$ we obtain an initial function corresponding to the exact self-similar solution (apart from a perturbation at the boundary). Then we solve problem (2.1) with this initial function and compare the results with the exact self-similar solutions (2.7).

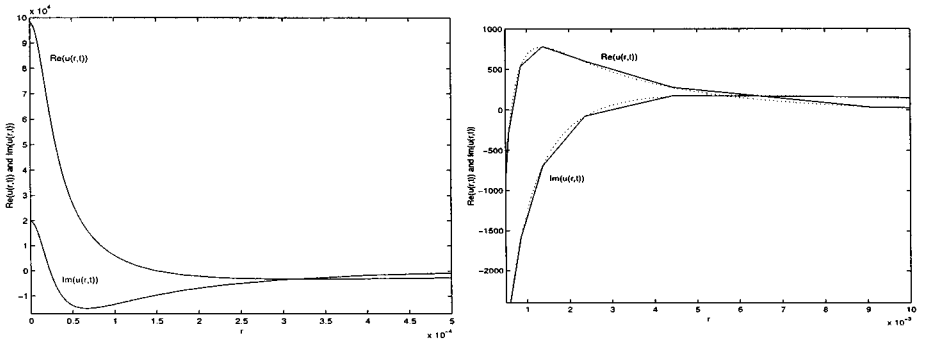

FIG. 5.8. $\mathrm{Re}(u(r,t))$ and $\mathrm{Im}(u(r,t))$ versus r for $t = 0.03430136123$ ($|u(0,t)| = 100{,}000$). The left figure is the leading part of solutions and the right figure is the middle part of solutions.

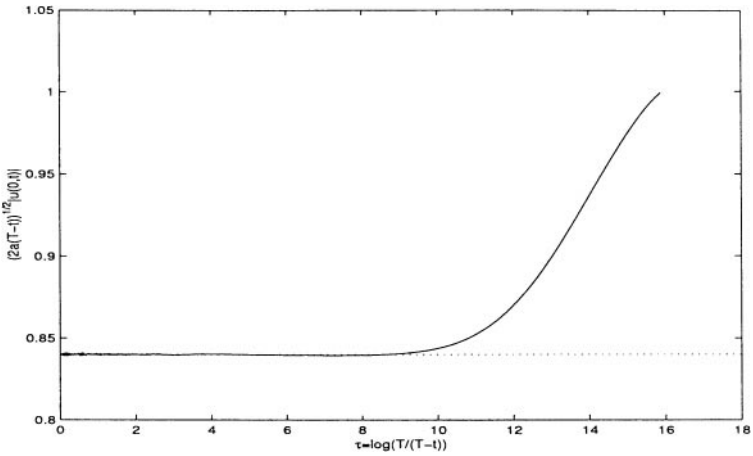

FIG. 5.9. $\sqrt{2a(T-t)}|u(0,t)|$ versus $\log(T/(T-t))$ for branch (0,1).

First, we consider the branch (0, 1) with $d=3$. On this branch, $a=0.3212$, $Q(0)=0.8399$, and hence

$$|u(0,0)| = 3.3137.$$

In Fig. 5.9 we plot the amplitude of the rescaled numerical solution $\sqrt{2a(T-t)}|u(0,t)|$. This clearly stays close to $Q(0)$ for some time before diverging, implying that the (0, 1) branch is mildly unstable. Indeed, $u(r,t)$ remains close to the self-similar solution at least until $|u(0,t)|=100$, retaining the multi-bump profile. In Fig. 5.10 we plot $|u(r,t)|$ against r for $|u(0,t)|=100$ ($t=0.09989$) and $|u(0,t)|=2500$ ($t=0.09999817$). The dotted line represents the exact self-similar solution (2.7) for the same time. In the latter figure it is clear that the multi-bump profile has evolved into the monotone profile characteristic of the blow-up profiles of the previous section.

Now we consider the branch (1, 2). For $d=3$ we have $a=0.2269$ and $Q(0)=1.1166$. We note that whereas the solution branch has 2 bumps for d close to 2, the solution at $d=3$ is monotone. In Fig. 5.11 we again plot the rescaled numerical solution at the origin and compare it with $Q(0)$. Again we see that the two solutions are initially close, but the (1, 2) solution is rather more unstable than the (0, 1) solution.

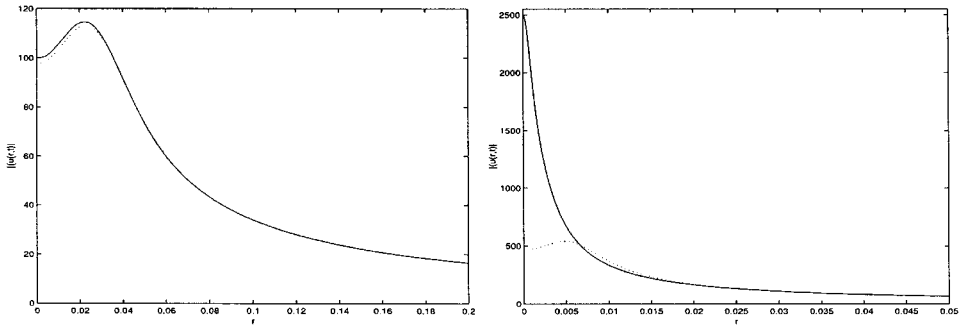

FIG. 5.10. $|u(r,t)|$ versus r for $|u(0,t)|=100$ on the left and for $|u(0,t)|=2500$ on the right.

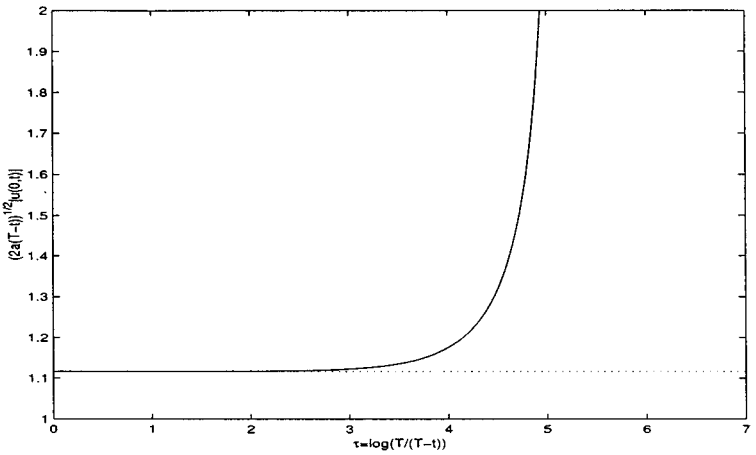

FIG. 5.11. $\sqrt{2a(T-t)}|u(0,t)|$ versus $\log(T/(T-t))$ for branch (1,2).

We conjecture that all of the further branches of self-similar solutions are unstable, with the degree of instability increasing with the number of bumps in the solution profile.

6. CONCLUSIONS AND FURTHER WORK

The results reported in this paper demonstrate that although the self-similar solution determined in [LPSS88a] is apparently globally attracting, it is not unique. Instead there are an infinite number of unstable self-similar solutions which bifurcate either from the ground state or from the zero solution when $d = 2$. The unstable self-similar solutions play a role in the transient dynamics of the evolution of the blow-up solutions and are thus worth studying in more detail. The scaling invariant numerical methods we have developed are effective in computing the dynamics of the solutions starting close to one of these self-similar states. In a future paper we will investigate their asymptotic properties as $d \to 2$ and will also consider the effect of using scaling invariant numerical methods in the special case of $d = 2$.

REFERENCES

[ACR81] U. Ascher, J. Christiansen, and R. D. Russell, Collocation software for boundary-value ODEs, *ACM Trans. Math. Software* **2**, 209 (1981).

[ADKM92] G. D. Akrivis, V. A. Dougalis, O. A. Karakashian, and W. R. McKinney, Galerkin-finite element methods for the nonlinear Schrödinger equation, in *Hellenic Research in Mathematics and Informatics 1992* (Hellenic Math. Soc., Athens, 1992), p. 421.

[BC98] C. J. Budd and G. C. Collins, Symmetry based numerical methods for partial differential equations, in *Numerical Analysis 1997, Proc. of 1997 Biennial Conference on Numerical Analysis*, edited by D. J. Higham, D. F. Griffiths, and G. A. Watson, Pitman Research Notes in Mathematics (Longman, Harlow/New York, 1998), p. 16.

[BCHR96] C. J. Budd, J. Chen, W. Huang, and R. D. Russell, Moving mesh methods with applications to blow-up problems for PDEs, in *Numerical Analysis 1995, Proc. of 1995 Biennial Conference on Numerical Analysis*, edited by D. F. Griffiths and G. A. Watson, Pitman Research Notes in Mathematics (Longman, Harlow/New York, 1996), p. 1.

[BHR96] C. J. Budd, W. Huang, and R. D. Russell, Moving mesh methods for problems with blow-up, *SIAM J. Sci. Comput.* **17**, 305 (1996).

[BCT96] B. Buffoni, A. R. Champneys, and J. F. Toland, Bifurcation and coalescence of a plethora of multi-modal homoclinic orbits in a Hamiltonian system, *J. Dynam. Differential Equations* **8**, 221 (1996).

[Bu83] T. A. Burton, *Volterra Integral and Differential Equations*, Mathematics in Science and Engineering (Academic Press, San Diego, 1983), Vol. 167.

[CT93] A. R. Champneys and J. F. Toland, Bifurcation of a plethora of multi-modal homoclinic orbits for autonomous Hamiltonian systems, *Nonlinearity* **6**, 665 (1993).

[DD87] E. A. Dorfi and L. O. Drury, Simple adaptive grids for 1-D initial value problems, *J. Comput. Phys.* **69**, 175 (1987).

[Fi96] G. Fibich, Adiabatic law for self-focusing of optical beams, *Opt. Lett.* **21**, 1735 (1996).

[FP98] G. Fibich and G. C. Papanicolaou, Self-focusing in the perturbed and unperturbed nonlinear Schrödinger equation in critical dimension, *SIAM J. Appl. Math.*, in press.

[Ha89] A. Hasegawa, *Optical Solitons in Fibers* (Springer-Verlag, Berlin, 1989).

[HR97] W. Huang and R. D. Russell, Analysis of moving mesh partial differential equations with spatial smoothing, *SIAM J. Numer. Anal.* **34**, 1106 (1997).

[HR96] W. Huang and R. D. Russell, A moving collocation method for time dependent partial differential equations, *Appl. Numer. Math.* **20**, 101 (1996).

[HRR94a] W. Huang, Y. Ren, and R. D. Russell, Moving mesh partial differential equations (MMPDEs) based on the equidistribution principle, *SIAM J. Numer. Anal.* **31**, 709 (1994).

[HRR94b] W. Huang, Y. Ren, and R. D. Russell, Moving mesh methods based upon moving mesh partial differential equations, *J. Comput. Phys.* **113**, 279 (1994).

[Ke93] H. Keller and G. Schroff, Stabilization of unstable procedures: The recursive projection method, *SIAM J. Numer. Anal.* **30**, 1099 (1993).

[KL95] N. Kopell and M. Landman, Spatial structure of the focusing singularity of the nonlinear Schrödinger equation: A geometrical analysis, *SIAM J. Appl. Math.* **55**, 1297 (1995).

[LPSS88a] B. J. LeMesurier, G. C. Papanicolaou, C. Sulem, and P. L. Sulem, Focusing and multi-focusing solutions of the nonlinear Schrödinger equation, *Phys. D* **31**, 78 (1988).

[LPSS88b] B. J. LeMesurier, G. C. Papanicolaou, C. Sulem, and P. L. Sulem, Local structure of the self-focusing singularity of the nonlinear Schrödinger equation, *Phys. D* **32**, 210 (1988).

[LPSS88c] M. J. Landman, G. C. Papanicolaou, C. Sulem, and P. L. Sulem, Rate of blowup for solutions of the nonlinear Schrödinger equation at critical dimension, *Phys. Rev. A* **38**, 3837 (1988).

[MPSS86] D. W. McLaughlin, G. C. Papanicolaou, C. Sulem, and P. L. Sulem, Focusing singularity of the cubic Schrödinger equation, *Phys. Rev. A* **34**, 1200 (1986).

[MS81] K. McLeod and J. Serrin, Uniquencess of solutions of semilinear Poisson equations, *Proc. Natl. Acad. Sci. U.S.A.* **78**, 6592 (1981).

[Pet82] L. R. Petzold, *A Description of DASSL: A Differential/Algebraic System Solver*, SAND82-8637, Sandia Labs, Livermore, CA, 1982.

[TS92] Y. Tourigny and J. M. Sanz-Serna, The numerical study of blowup with application to a non-linear Schrödinger equation, *J. Comput. Phys.* **102**, 407 (1992).

[W90] X. P. Wang, *On Singular Solutions of the Nonlinear Schrödinger and Zakharov Equations*, Ph.D. thesis, New York University, 1990.

[Za84] V. E. Zakharov, *Handbook of Plasma Physics*, edited by M. N. Rosenbluth and R. Z. Sagdeev (Elsevier, New York, 1984), Vol. 2.